Warsaw University of Technology

Faculty of Power and Aeronautical Engineering

Finite element analysis of an elastomeric artificial disc in lumbar spine

Study of a parametric artificial intervertebral disc under different load states and positions in the lumbar spine

Oleguer Sans i Ballart

Tutor: Paweł Borkowski

July 2011

Index

Abstract

The main objective of this project is to make a parametric design of an intervertebral artificial lumbar disc using FE software (ANSYS) in APDL language (ANSYS parametric design language) and then use that software to study the structural response of the intervertebral disc in different situations. First of all the functions of the real intervertebral disc and its structure are going to be exposed, then continue with the explanation of the intervertebral artificial disc and its parameters. After the explanation modified artificial disc with thicker brim inlay is going to be analyzed under different loads studying its response. Then the disc is going to be inserted in the intervertebral space (L4-L5) of a model of the lumbar spine and it is going to be analyzed under a normal and a combined (vertical and horizontal) load state in two different positions, the correct one and a wrong one.

Functions of the real intervertebral disc

The vertebral spine is made of Intervertebral discs, vertebrae and ligaments, all these structures are passive elements of the musculoskeletal system. The spinal column movements occur as a combination of several segments movements. These segments that allow the spinal movement are the vertebrae, the intervertebral discs, the anterior and posterior longitudinal ligaments and the vertebral joints. The combined movement of all these segments allows the spine to get a great flexibility as a whole. The discs adapt to the spinal movements as best as possible, the properties of the nucleus pulposus and the annulus fibrosus, allows turning the movements of the spine to smoother ones. The nucleus pulposus acts as an incompressible pillow of water. The center of a healthy disc (nucleolus pulposus) is centered when the spine is in its rest position and during the movement it moves outward. The annulus fibrosus guides the nucleus pulposus during this movement. Vertical loads of the spine are absorbed by the discs. In fact the intervertebral discs are the perfect shock absorbers because they are capable of snapping back into its place and they can adjust to several kinds of movements.

Description of the intervertebral disc

The intervertebral disc (*fig. 1*) is an elastic structure of elastic annular fibers made of mucopolysaccharides. The fibers may be lined up like strands of nylon rope or crisscrossed like a net. An intervertebral disc is made of three parts; the center, called the nucleus pulposus, the annulus fibrosus that surrounds the nucleus pulposus and the vertebral end-plates.

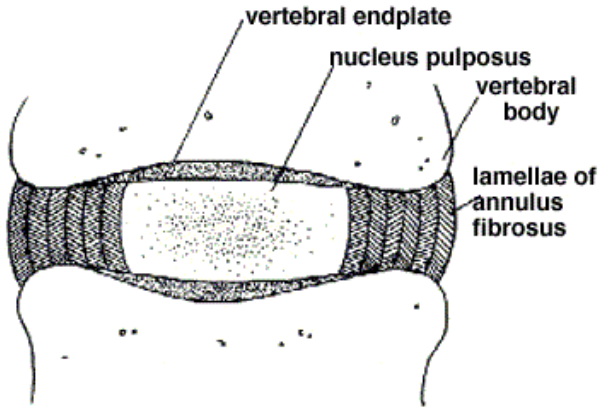

Figure 1: Sagittal view of the intervertebral disc with its structures [1]

The nucleus pulposus located in the centre of the disc. In young and healthy people, this material is a gel made of an 88%[1] of water therefore highly hydrophilic. Because the disc core is a fluid, it can be deformed but not compressed. When a compressive load is applied to the intervertebral disc, it changes its shape without a reduction of its total volume. By changing its shape, the nucleus generates hydraulic pressure which is held by the annulus fibrosus. In a neutral position, the intervertebral disc transforms vertical to radial forces (*fig. 2*).

The annulus fibrosus (*fig. 3*) is a 10-20 densely packed concentric rings of collagen fiber strands

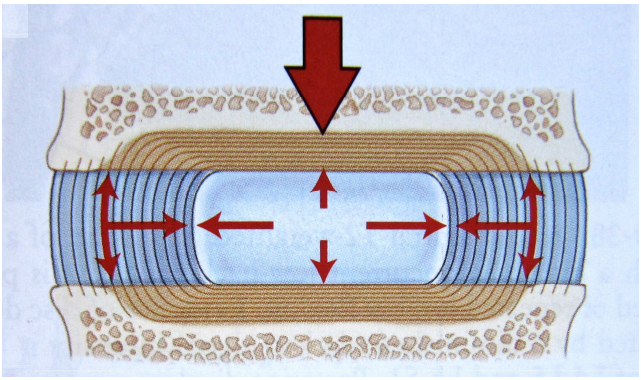

Figure 2: Vertical loads are transformed to hydraulic pressures [2]

(lamellae) that surround and contain the liquid nucleus whose obliquity is crossed when moving from one layer to the next. The collagen fibers arrange themselves in a fixed pattern: their direction alternates in successive rings from left to right, always maintaining an orientation of about 65 degrees off vertical.

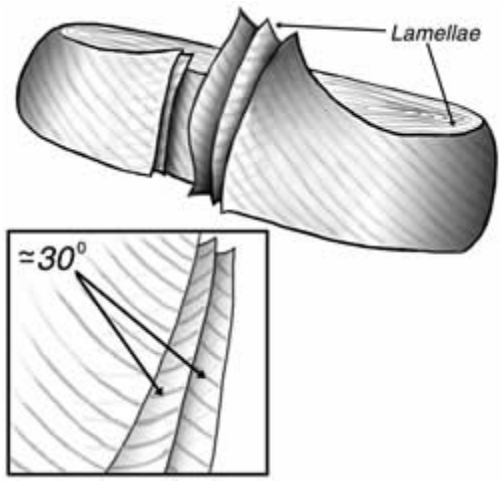

Figure 3: The angle of the fibbers between two consecutive layers is about 30 degrees [3]

In both top and bottom of each vertebra there is a 0.75 mm of cartilaginous pad called the vertebral end-plate. These end-plates are not attached to the subchondral bone of the

[1] *Fisiologia articular: Tronco y raquis.* A.I. KAPANDJI, Editorial Medica Panamericana. 1998

vertebrae but are instead strongly interwoven into the annulus of the disc. Because its morphological similarities the vertebral end-plates are considered part of the disc.

Structure of the artificial intervertebral disc

This artificial intervertebral lumbar disc (*fig. 4*) is made of three differentiated parts, two of them are metal plates, that are going to be fixed to the vertebrae (L4-L5 or L5-S1), and the other one which is made of an hyperelastic material that is the one that actually simulate the structural functions of the intervertebral disc.

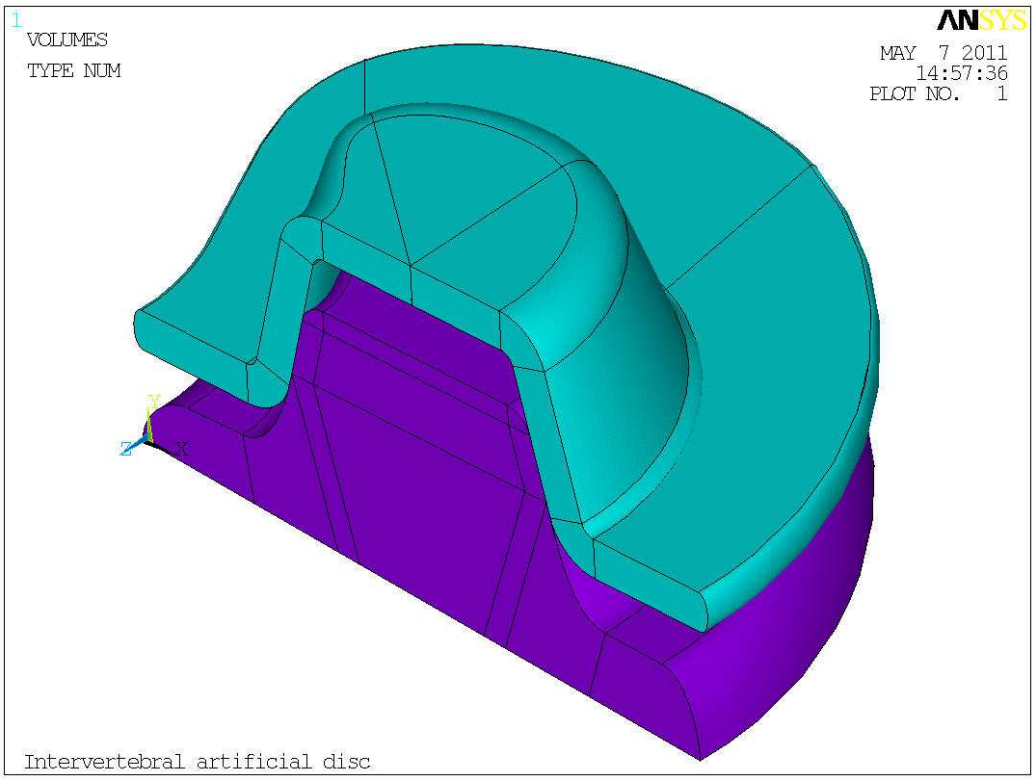

Figure 4: View of a quarter of the artificial disc (blue volumes are the metal plate and purple volumes are the hyperelastic inlay)

The intervertebral artificial disc must work as similar as the real intervertebral disc; it means that has to resist the compressive and the shear loads that are usually applied to the real intervertebral disc. As it can be observed in the picture, this model has two symmetry planes.

Parameters of the artificial intervertebral disc

One of the most important aspects of this design are the parameters, they are used to provide the best adjustment to the patients anatomy. The following pictures (*figs. 5 & 6*) show the parameters of the metal plates (blue bodies in the *fig. 4*) of the artificial intervertebral disc.

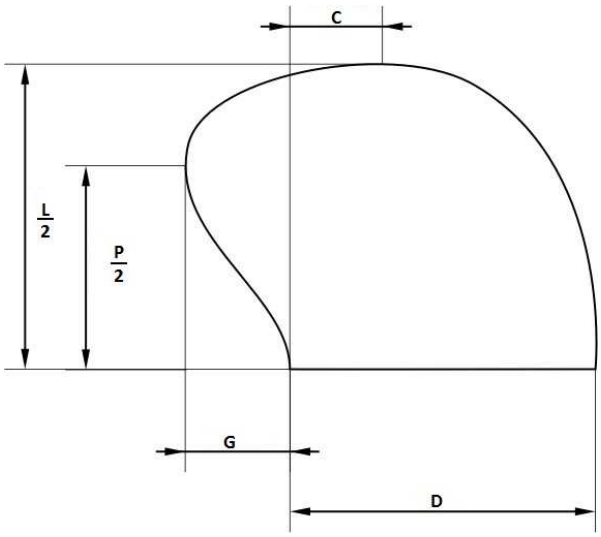

Figure 5: Upper view of the plate of the artificial intervertebral disc with its parameters.

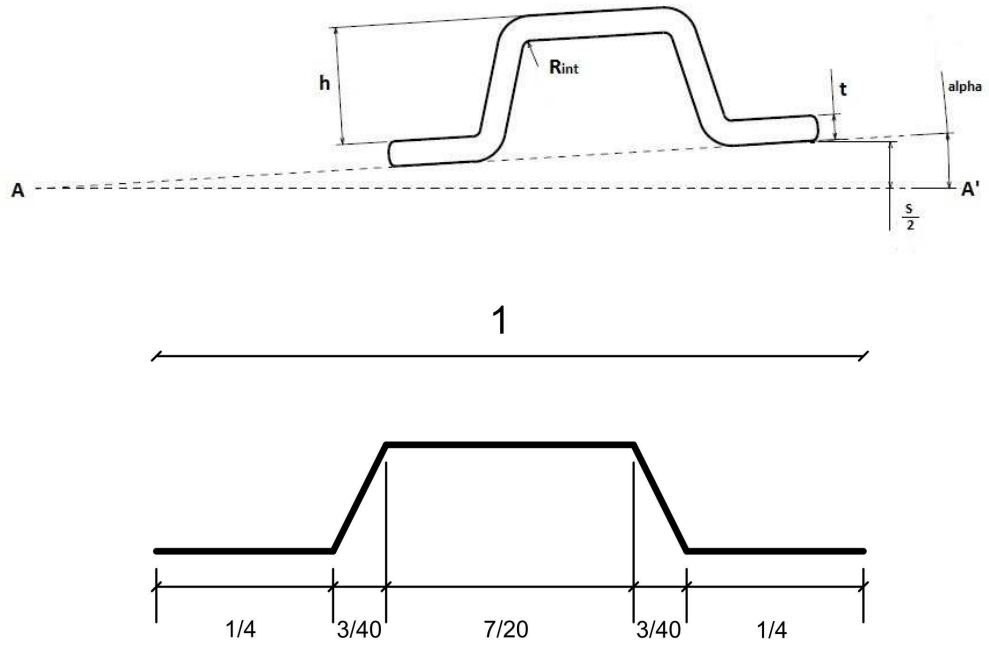

Figure 6: Sagittal view of the plate of the artificial intervertebral disc with its parameters and ratios

Where *L* is the width of the vertebral endplate, *G* is the depression in the vertebral body produced by the vertebral foramen, *P* is the distance between the outer parts of back

vertebral body, *c* is the horizontal distance from the lateral external side of the vertebrae to the inner depression of the vertebral body produced by the vertebral foramen, *D* is the distance from the front to the back side of the vertebral body. In the sagittal view of the intervertebral artificial disc plate, *h* would be the deepness of the hole made into the vertebral body to fit the intervertebral artificial disc, *t* is the thickness of the metal plate, R_{int} is the radius of the small radius over all the plate, it means the inner one and the outer one. About the outer radius its value is the sum of R_{int} and the thickness of the plate. *Alpha* is the half angle between the two adjacent vertebrae, *S* is the greatest vertical distance between the two adjacent vertebrae and finally the line A-A' defines the midplane of the intervertebral artificial disc. To generate the socket shape, the ratios from the *figure 6* have to be multiplied by the parameter D. The upper areas of the metal plates are proportional to the shape of the *figure 5* according to the ratios of the *figure 6*.

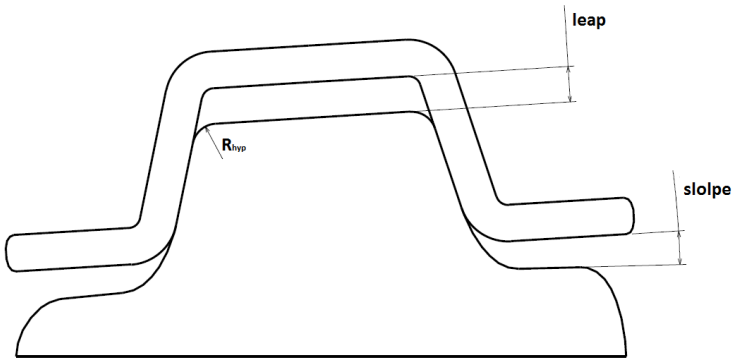

Figure 7: Sagittal view of the hyperelastic inlay with its parameters.

In the parametric design of the inlay there are less parameters than in the metal plates because most of its geometric constrains are based on relations with the metal plates. In the previous picture (*fig. 7*), R_{hyp} is the edge radius of the part of the hyperelastic inlay that fits into the plate socket, the *slope* is the angle between the metal plate and the brim of the hyperelastic inlay and the last one is called *leap* which is the distance between the plate socket and the hyperelastic inlay that fits in it.

All this parameters give us the chance to create thousands of different artificial intervertebral discs. To show the possibilities of the parametric design, some of the multiple possible shapes of the artificial intervertebral discs are going to be shown with its parameters (*fig. 8*).

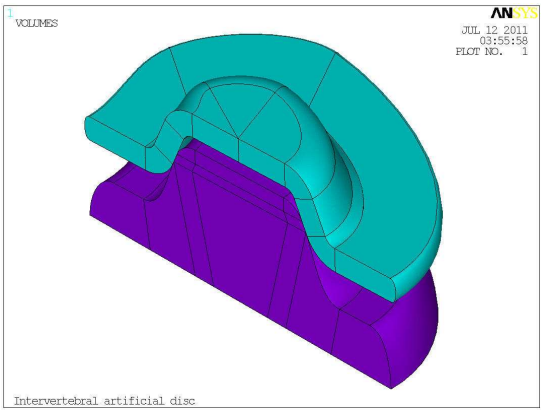

Model #1		P	20 mm
S	15 mm	G	2 mm
alpha	2°	c	7 mm
D	30 mm	R_{int}	1 mm
h	5 mm	leap	1 mm
t	2 mm	slope	0°
L	35 mm	R_{hyp}	2 mm

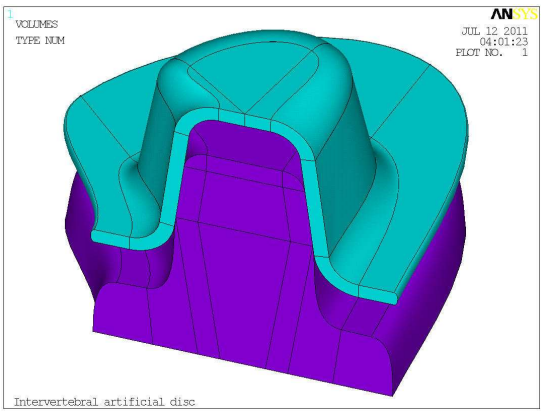

Model #2		P	25 mm
S	15 mm	G	5 mm
alpha	0.5°	c	15 mm
D	20 mm	R_{int}	2 mm
h	12 mm	leap	3 mm
t	1 mm	slope	2°
L	45 mm	R_{hyp}	1.5 mm

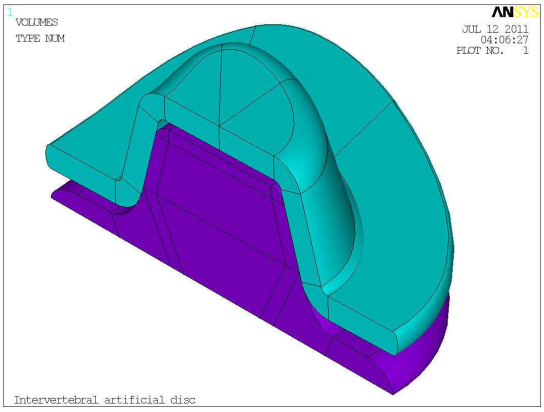

Model #3		P	30 mm
S	5 mm	G	0 mm
alpha	1.5°	c	10 mm
D	25 mm	R_{int}	0.5 mm
h	7 mm	leap	0.5 mm
t	1.5 mm	slope	1°
L	30 mm	R_{hyp}	1 mm

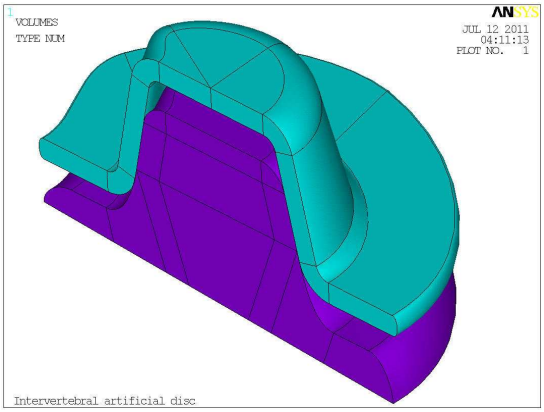

Model #4		P	20 mm
S	10 mm	G	3 mm
alpha	3.5°	c	12 mm
D	30 mm	R_{int}	1 mm
h	10 mm	leap	2 mm
t	1.5 mm	slope	0°
L	35 mm	R_{hyp}	2 mm

Figure 8: Several parametric models of the prosthesis

Parametric design of the artificial intervertebral disc

The intervertebral artificial disc model has been built using the "bottom up" construction method (*fig. 9*), it means that at first simple entities are defined and from these more complex entities are defined. Using this method first of all keypoints are defined as the vertices of the volumes, lines are defined using these keypoints, areas are defined using the previous lines and finally volumes are defined using the areas.

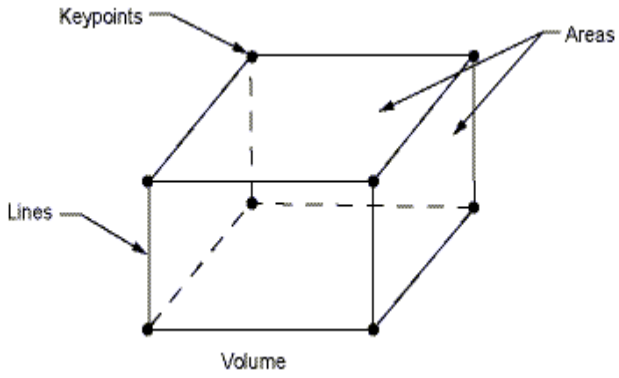

Figure 9: "Bottom up" construction [4]

Parametric design means that by defining a set of main parameters of the model, the other parameters are defined as a mathematical combination of the main parameters. The APDL code that defines this model allows the user to change the values of the design parameters during the execution of the code. It is important to know that all the parameters have its units; distances are defined in millimeters and angles in degrees. It is also important to know that the design have its own limitations, not any value of the parameters can be introduced because there could be geometrical incompatibilities, so all the parameters values have to be coherent.

Modeling of the artificial intervertebral disc

The metal plates of the artificial intervertebral are made of metallic alloy Co-Cr-Mo, it has been modeled with a modulus of elasticity of $E = 2.1 \cdot 10^5 \mathrm{MPa}$ and a Poissons ratio of $\nu = 0.3$. Moreover the hyperelastic inlay is made of an elastomer material. The inlay is made of an incompressible material, it means that its Poissons ratio is $\nu = 0.5$, in this case the relation between the shear modulus and the modulus of elasticity is $E = 3G$. One important effect that has to be considered is the contact between the metal plates and the hyperelastic inlays, in this case the coefficient of friction between both materials is $\mu = 0.05$.

Metal plates

Two material models are going to be used in the analysis; the first one is the elastic linear material model and corresponds to the metal plates. Considering this kind of model, the material behavior will be the following (without considering the effects of temperature):

- The specimen deforms reversibly: If you remove the loads, the solid returns to its original shape.
- The strain in the specimen depends only on the stress applied to it - it doesn't depend on the rate of loading, or the history of loading.
- For most materials, the stress is a linear function of strain, because the strains are small, this is true whatever stress measure is adopted and is true whatever strain measure is adopted.
- For most, but not all, materials, the material has no characteristic orientation. Thus, if you cut a tensile specimen out of a block of material, the stress-strain curve will be independent of the orientation of the specimen relative to the block of material. Such materials are said to be isotropic.

The formulation of this model is based on the Hooke's Law equation, using index notation it looks like the following:

$$\varepsilon_{ij} = \frac{1+\nu}{E}\sigma_{ij} - \frac{\nu}{E}\sigma_{kk}\delta_{ij}$$

Where $\sigma_{kk} = \sigma_{xx} + \sigma_{yy} + \sigma_{zz}$, and δ_{ij} is the Kronecker delta, defined as:

$$\delta_{ij} = \begin{cases} 1, & i = j \\ 0, & i \neq j \end{cases}$$

In the matrix notation it looks like:

$$\begin{bmatrix} \varepsilon_{xx} \\ \varepsilon_{yy} \\ \varepsilon_{zz} \\ \varepsilon_{xy} \\ \varepsilon_{xz} \\ \varepsilon_{yz} \end{bmatrix} = \frac{1}{E}\begin{bmatrix} 1 & -\nu & -\nu & 0 & 0 & 0 \\ -\nu & 1 & -\nu & 0 & 0 & 0 \\ -\nu & -\nu & 1 & 0 & 0 & 0 \\ 0 & 0 & 0 & (1+\nu) & 0 & 0 \\ 0 & 0 & 0 & 0 & (1+\nu) & 0 \\ 0 & 0 & 0 & 0 & 0 & (1+\nu) \end{bmatrix}\begin{bmatrix} \sigma_{xx} \\ \sigma_{yy} \\ \sigma_{zz} \\ \sigma_{xy} \\ \sigma_{xz} \\ \sigma_{yz} \end{bmatrix}$$

One of the multiple ANSYS elements that can simulate linear isotropy, and the one that is going to be used, is the SOLID45 (*fig. 10*). This element is used for the 3-D modeling of solid

structures; it is defined by eight nodes having three degrees of freedom at each node: translations in the nodal x, y and z directions.

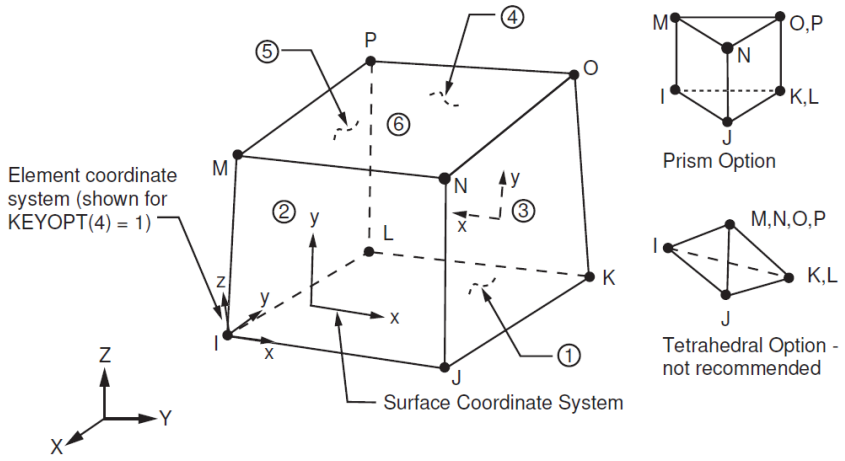

Figure 10: Geometry of the element SOLID45 [5]

The geometry, node locations and the coordinate system for this element are shown in the previous figure. This element is defined by eight nodes and the orthotropic material properties. Orthotropic material directions correspond to the element coordinate directions.

Hyperelastic inlay

In the other hand, the other material model is called Gent (*fig. 11, blue sky line*) and it is the one that correspond to the hyperelastic inlay. According to the information given by the Chapter 6 (Hyperelasticity) of ANSYS Workbench – Mechanical Structural Nonlinearities[2], the hyperelastic inlay is an elastomer (also knew as rubber) material and some of their particular properties must be known:

- Elastomers are natural and synthetic polymers which are amorphous. They are made of long cross-linked molecular chains.
- These molecular chains are highly twisted and coiled, with a random orientation.
- Under a tensile load, these chains become partially straightened and untwisted.
- When the load is removed, the chains return to their initial configuration.
- By the vulcanization process, the rubber is strengthened by forming crosslinks between molecular chains.

[2] *www.cadfamily.com/download/CAE/ANSYS-Multiphysics/Hyper.ppt*

On a macroscopic level, rubber behavior exhibits certain characteristics (*fig. 11*):

- They can be highly deformed, from 100 to 700%, recovering their initial configuration. This behavior is due to the untwisting of the cross-linked molecular chains.
- The small change of volume under applied stress is due the straightening of molecular chains; according to this elastomers are nearly incompressible.
- The stress-strain relationship can be highly nonlinear.
- In tension, the material softens and in compression, the response becomes quite stiff.

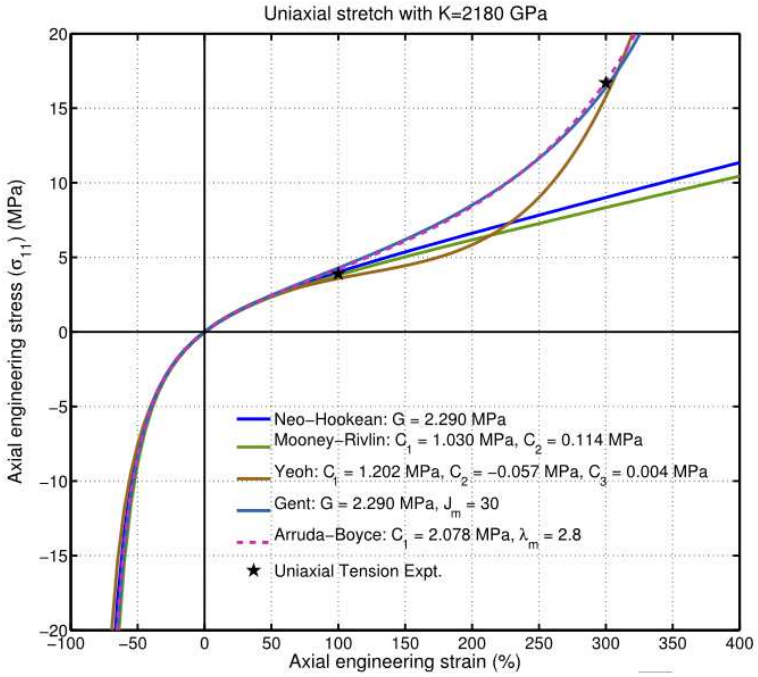

Figure 11: Strain-stress graphic of some hyperelastic material models under uniaxial load [6]

When using hyperelastic models in ANSYS there are some assumptions that must be known; material response is isotropic, isothermal and elastic, and also the material is fully or nearly incompressible. In the current case, it is not possible to use the Hooke's law like in the linear elastic model, in hyperelastic models, total stress vs. total strain is defined through a strain energy potential (W).

Before proceeding to a detailed explanation of the Gent strain energy potential, some terms will be defined. The stretch ratio (or stretch) is defined as:

$$\lambda = \frac{L}{L_0} = \frac{L_0 + \Delta u}{L_0} = 1 + \varepsilon_E$$

The previous expression is an example of stretch ratio defined for uniaxial tension of an elastomer where ε_E is engineering strain. There are three principal stretch ratios λ_1, λ_2 and λ_3 which provide a measure of the deformation. These will also be used in defining the strain energy potential.

To illustrate the definition of the principal stretch ratios, consider a thin square rubber sheet in biaxial tension (*fig. 12*). The principal stretch ratios λ_1 and λ_2 characterize the plane deformation. On the other hand, λ_3 defines the thickness variation (t/t_0). If it is assumed that the material is fully incompressible, λ_3 will equal λ^{-2}.

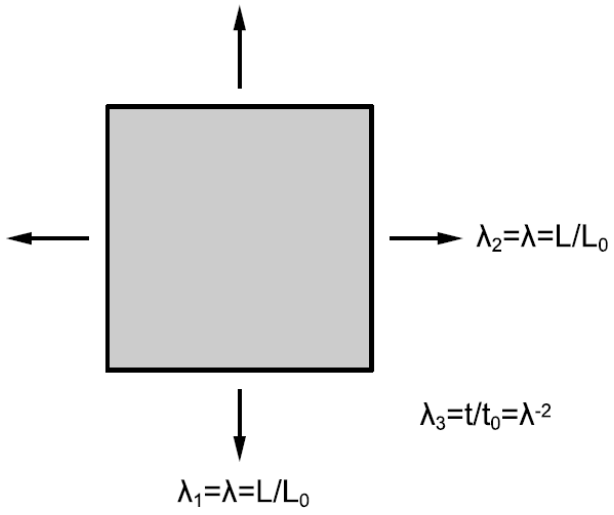

Figure 12: Square rubber sheet in biaxial tension

The three strain invariants are used to define the strain energy density function:

$$I_1 = \lambda_1^2 + \lambda_2^2 + \lambda_3^2$$

$$I_2 = \lambda_1^2\lambda_2^2 + \lambda_2^2\lambda_3^2 + \lambda_3^2\lambda_1^2$$

$$I_3 = \lambda_1^2\lambda_2^2\lambda_3^2$$

If the material is fully incompressible, $I_3 = 1$.

Because we assume that the material is isotropic, some forms of strain energy potential are expressed as a function of these scalar invariants. Strain invariants are measures of strain which are independent of the coordinate system used to measure the strains.

The volume ratio is defined as:

$$J = \lambda_1\lambda_2\lambda_3 = \frac{V}{V_0}$$

As shown above, J can be thought of as the ratio of deformed to undeformed volume of the material.

Strain energy potential can be defined as a direct function of the principal stretch ratios or a function of the strain invariants:

$$W = W(I_1, I_2, I_3) \quad \text{or} \quad W = W(\lambda_1, \lambda_2, \lambda_3)$$

Based on W, second Piola-Kirchoff stresses (and Green-Lagrange strains) are determined:

$$S_{ij} = \frac{dW}{dE_{ij}}$$

Because of material incompressibility, we can split the W expression as the sum of the deviatoric (subscript d or with 'bar') and volumetric (subscript b) terms. As a result, the volumetric term is a function of J only.

$$W = W_d(\bar{I}_1, \bar{I}_2) + W_b(J)$$
$$W = W_d(\bar{\lambda}_1, \bar{\lambda}_2, \bar{\lambda}_3) + W_b(J)$$

The deviatoric principal stretches and invariants are defined as (for $p = 1, 2, 3$):

$$\bar{\lambda}_p = J^{-1/3}\lambda_p$$
$$\bar{I}_p = J^{-2/3}I_p$$

There is no need to use I_3 to define W because $I_3 = J^2$.

As it has been commented before, the hyperelastic inlay is modeled using the Gent model. The Gent model is a micromechanical model which utilizes the concept of limiting network stretch:

$$W = \frac{EI_m}{6}\ln\left(1 - \frac{\bar{I}_1 - 3}{I_m}\right) + \frac{1}{d}\left(\frac{J_{el}^2 - 1}{2} - \ln J_{el}\right)$$

Where the constants E, I_m and d are input. E is the initial elastic modulus, which for incompressible materials is $3\mu_0$, where μ_0 is the shear modulus (also named G). I_m is the limiting value of $(I_1 - 3)$ and d is the material incompressibility. In our inlay model, the input values are the following:

$$\mu_0 = 5\ MPa$$

$$I_m = 80$$

$$d = 0\ MPa^{-1}$$

In the case of $d = 0\ MPa^{-1}$, ANSYS ignores the second term of the strain energy function.

The ANSYS element that is going to be used with the Gent model is the SOLID185 (*fig. 13*). This element is geometrically equal to the SOLID45 but its difference is that it is possible to use the Gent model with it.

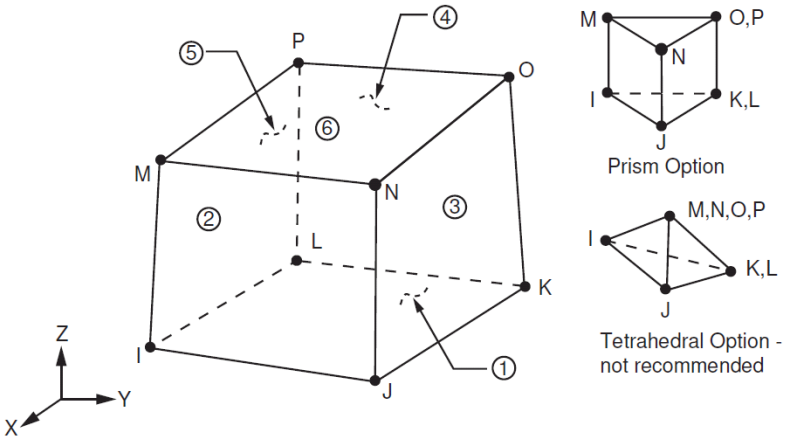

Figure 13: Geometry of SOLID185 [5]

SOLID185 is used for 3-D modeling of solid structures. It is defined by eight nodes having three degrees of freedom at each node: translations in the nodal x, y and z directions. It has a formulation for simulating deformations of nearly incompressible elastoplastic materials and fully incompressible hyperelastic materials among others. This element can be used as a homogeneous structural solid, which is the one that is going to be used, and as a layered structural solid.

Contacts

Because the plates and the inlay touch each other, the inlay is going to get deformed and because of this, new stresses are going to appear. The simplest way to model it, is using the Pure Penalty Method. According to the information given by Erke Wang – ANSYS contact[3], this method requires both contact normal (ε_N) and tangential stiffness(ε_T). Both surfaces have to be defined, one of them is going to be the contact surface, and the other one the target surface. This difference is because the surface called target (which is the most deformable) will cross the so called target surface (which is the stiffest).

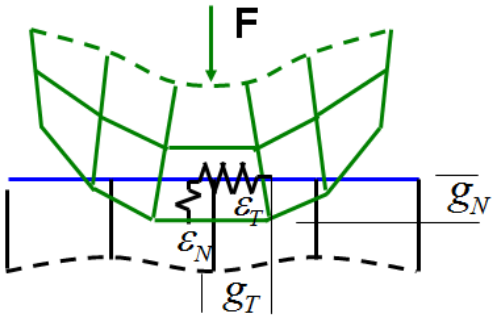

Figure 14: Contact (blue) and target surface (green) [7]

The main drawback is that the amount penetration between the target and the contact surface depends of their stiffness (*fig. 14*). In this method, penalty means that any violation of the contact condition will be punished by increasing the total virtual work. In FE form this method is defined like:

$$(K + \varepsilon G^T G)u = F$$

Where ε is the contact stiffness. The contact spring will deflect an amount Δ, such that equilibrium is satisfied:

$$\varepsilon\Delta = \mathrm{F}$$

Some finite amount of penetration, $\Delta > 0$, is required mathematically to maintain equilibrium. However, physical contacting bodies do not interpenetrate ($\Delta = 0$).

The ANSYS elements that are going to be used to model the contacts are called CONTA174 and TARGE170. Both of them are used to describe the boundary of the volumes that are going to touch each other. As its name suggests, CONTA174 is used to define the contact surface and the element TARGE170 defines the target area.

[3] http://www.scribd.com/doc/36284870/Erke-Wang-Ansys-Contact

CONTA174 has the same geometric characteristics as the solid or shell element face with which it is connected. Contact occurs when the element surface penetrates one of the target segment elements on a specified target surface. Coulomb and shear stress friction is allowed.

The contact elements themselves overlay the solid describing the boundary of a deformable body and are potentially in contact with the target surface, defined by TARGE170. This target surface is discretized by a set of target segment elements and is paired with its associated contact surface via a shared real constant set.

Compression loads over the disc

Compression loads over the disc are more important as we approach to the sacrum. This is because as we move down, the body weight increases. In the case[4] of a man of 80 kg, it is assumed that his head weight 3 kg, the arms 14 kg and his torso 30 kg. If we assume that the disc between L5 and S1 supports only 2/3 of the torso, a load of 37 kg is reached, about half of the body weight. If we consider[5] a disc under a load of 40 kg, we can observe that it is flattened 1 mm and at the same time it widens 0.5 mm.

The previous values are going to be useful to compare the results of the analysis of the artificial intervertebral disc.

[4] *Fisiologia articular: Tronco y raquis.* A.I. KAPANDJI, Editorial Medica Panamericana. 1998

[5] BOGDUK, N.; ENDRES, S.M. (2005). *Clinical Anatomy of the Lumbar Spine and the Sacrum.* 4th ed. Churchill Livingstone, ISBN: 0-443-10119-1

Artificial disc structural response

To study the response of the intervertebral artificial disc and its influence to the surrounding structures, it is going to be tested under different situations. First of all, it s going to be tested alone applying a descending displacement of 2 mm to the upper plate and also applying a horizontal displacement to the upper plate of 2 mm in the sagittal plane.

Control analysis under compression

The first study is going to be a control analysis under compression of the intervertebral artificial disc (*fig. 15*). In this case, the upper side of the plate has been forced to displace 2 mm down. This analysis is going to be useful because it will show the stress response of the disc under a pure compression load. The boundary conditions of this analysis are simply applied to the areas defined by the symmetry planes. The areas defined by the sagittal plane are constricted in the Z direction and the areas defined by the horizontal plane are constricted in the Y direction. It can be expected that the higher stresses are going to be found in the plate because the hyperelastic inlay is going to make pressure against the socket. One of the values that must be considered, is the vertical reaction according to the vertical displacement, in this case, because the model is divided by the sagittal plane, the value of the vertical reaction that ANSYS show is going to be the half value of the real one, on the other hand, because its boundary conditions are symmetric its real displacement is the double of the applied one.

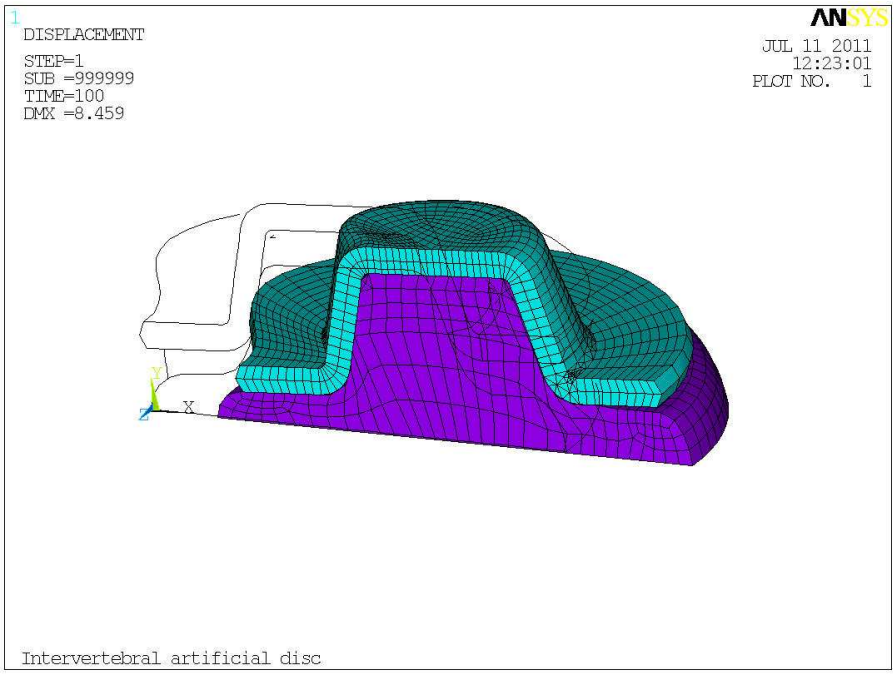

Figure 15: Deformed shape of the intervertebral artificial disc under compression

Because of the different stiffness of the materials involved into the analysis, the stresses of the plate and the inlay are going to be shown by separate. Because of its stiffness, the stresses of the metal plates are going to be much greater than the ones from the inlay, and if they are shown together, the higher values of the plate's stresses are going to hide the lower stresses of the inlay.

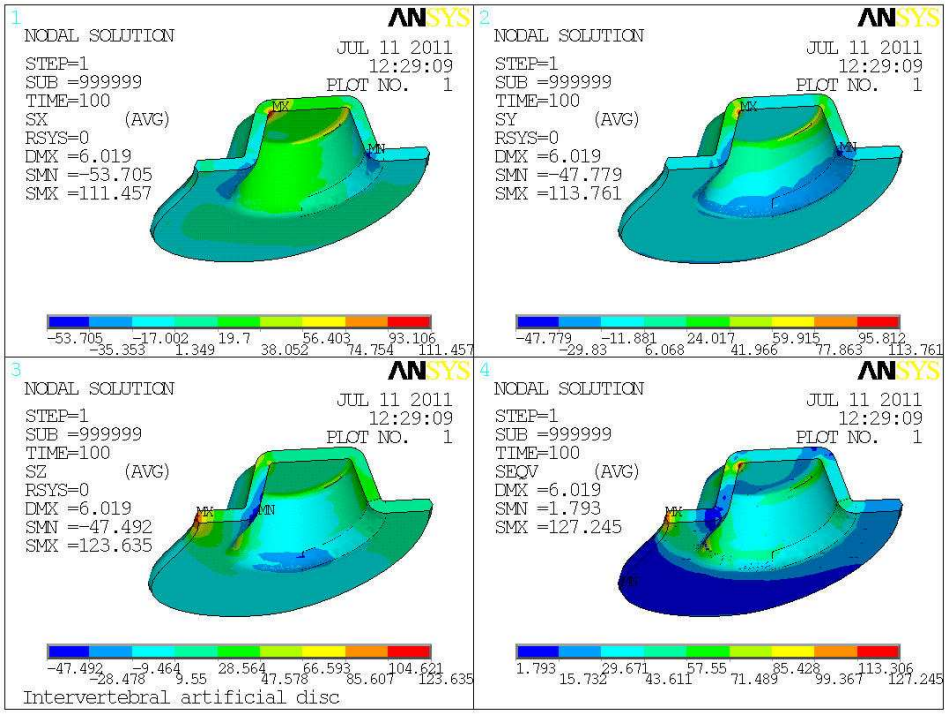

Figure 16: Sx, Sy, Sz and Seqv of the plate.

If an infinitesimal volume is considered and this volume is in a coordinate system, σ_x, σ_y and σ_z (Sx, Sy and Sz in ANSYS) are the normal stresses of the volume according to the coordinate system (*fig. 18*).

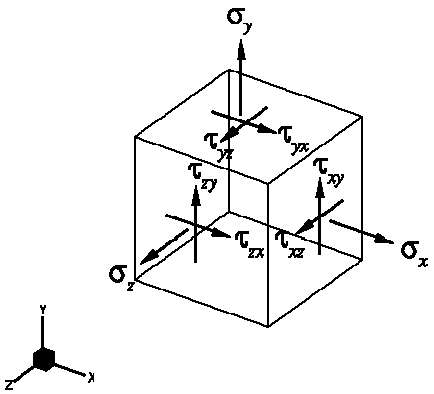

Figure18: Infinitesimal volume with its stresses and coordinate system [8]

There is a particular coordinate system where all the stresses are perpendicular to the faces of the infinitesimal volume; it means that there are not shear stresses. In this particular coordinate system the stresses are called principal stresses σ_1, σ_2 and σ_3. This principal stresses are displayed in descending order $\sigma_1 > \sigma_2 > \sigma_3$. Finally, Von Mises stress (Seqv in ANSYS) is defined as:

$$\sigma_e = \left(\frac{(\sigma_1 - \sigma_2)^2 + (\sigma_2 - \sigma_3)^2 + (\sigma_3 - \sigma_1)^2}{2} \right)^{1/2}$$

As we can observe in the previous images (*fig.16*), the greater stresses are localized on the edges of the interior of the plate.

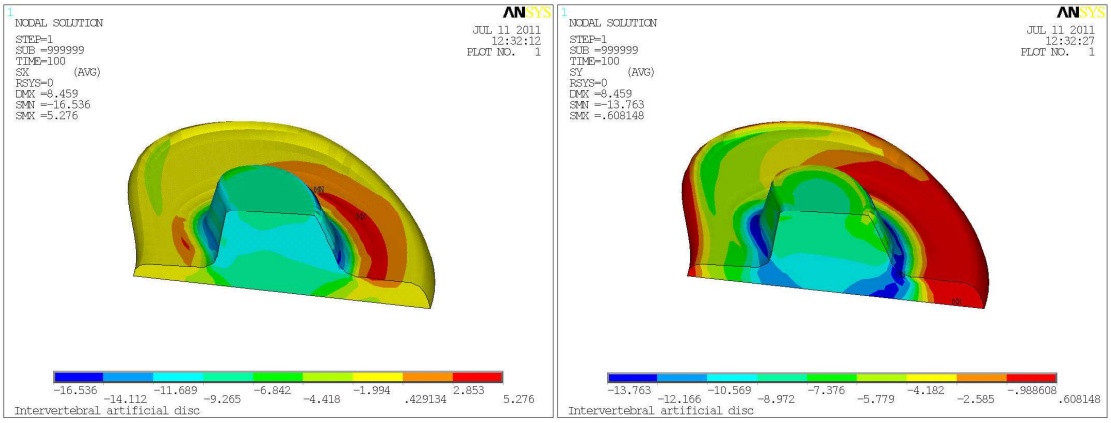

Figure 17: Sx and Sy of the inlay

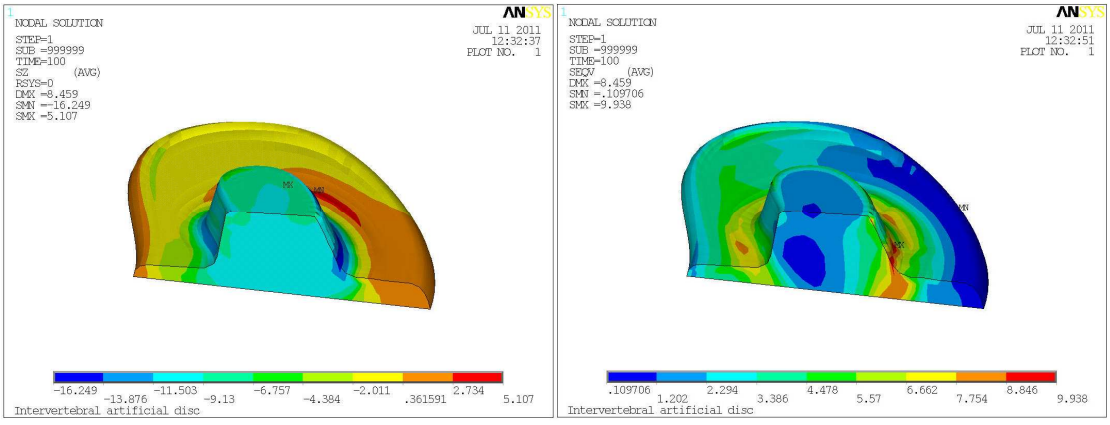

Figure 18: Sz and Seqv of the inlay

As it can be observed in the images (*figs. 17 & 18*), greater efforts are found in the zones where there is the contact between the metal plate and the inlay. It is remarkable that the maximum compressive stresses are localized in the contact between the edge of the socket and the inlay.

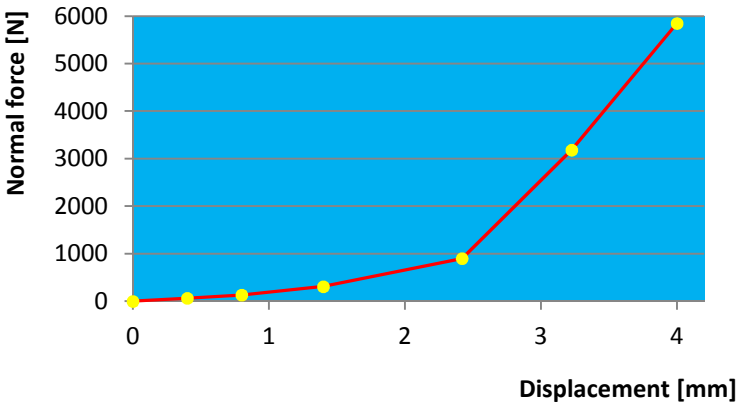

Figure 19: Normal force vs. displacement curve of the disc under normal load

The previous graphic (*fig. 19*) shows the response of the disc under the normal load of compression. At the beginning of the compression the artificial intervertebral disc is easily deformable, but when the compression is considerable, it is more difficult to continue deforming it. As the disc is compressed, its stiffness increases, this is why it is necessary more load to deform it. As it was mentioned before, the graphic shows the real displacement and loads of the intervertebral artificial disc which is the double distance and double load that were shown by the ANSYS software.

Control analysis under shear load

In this case, a horizontal displacement of 2 mm is applied to the intervertebral artificial disc in the anterior direction (*fig. 20*). This analysis will be useful to obtain the disc response under a pure shear load, it is also important because one of the most common injuries, spondylolisthesis, is produced by loads of this nature. In this case we are going to work with the half of the prosthesis. The nodes from the upper areas of the upper plate are going to be forced to move 2 mm to the anterior direction and their vertical movement is going to be constrained, the nodes from the lower areas of the lower plate are going to be all constrained and finally, the movement in the Z direction of the areas of the sagittal plane is going to be constrained.

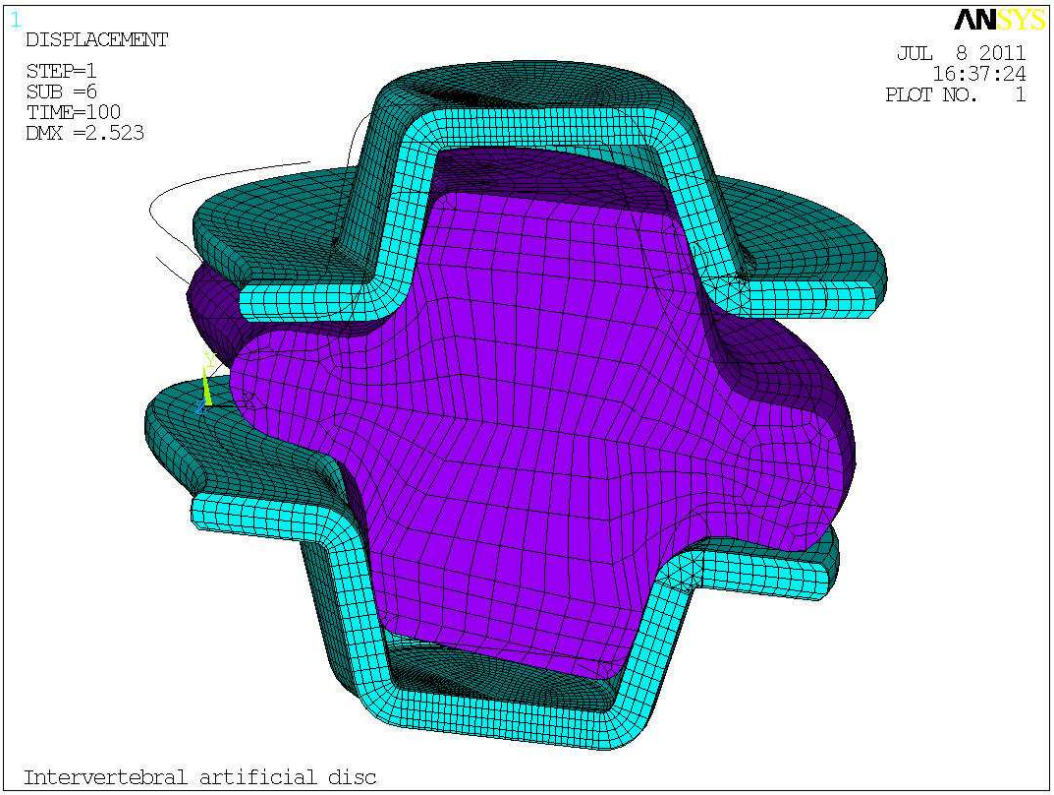

Figure 20: Deformed shape of the intervertebral artificial disc under shear load

According to the previous reasons, the stresses of the plate and the inlay are going to be displayed by separate. Like in the previous case, pure compression, the results are not going to match with the real ones because in this case only the intervertebral artificial disc is studied, in the real case, the intervertebral disc is surrounded by other structures like ligaments, muscles and the vertebral processes. All these structures absorb part of the load reducing the total load applied to the intervertebral disc and therefore limiting its displacement.

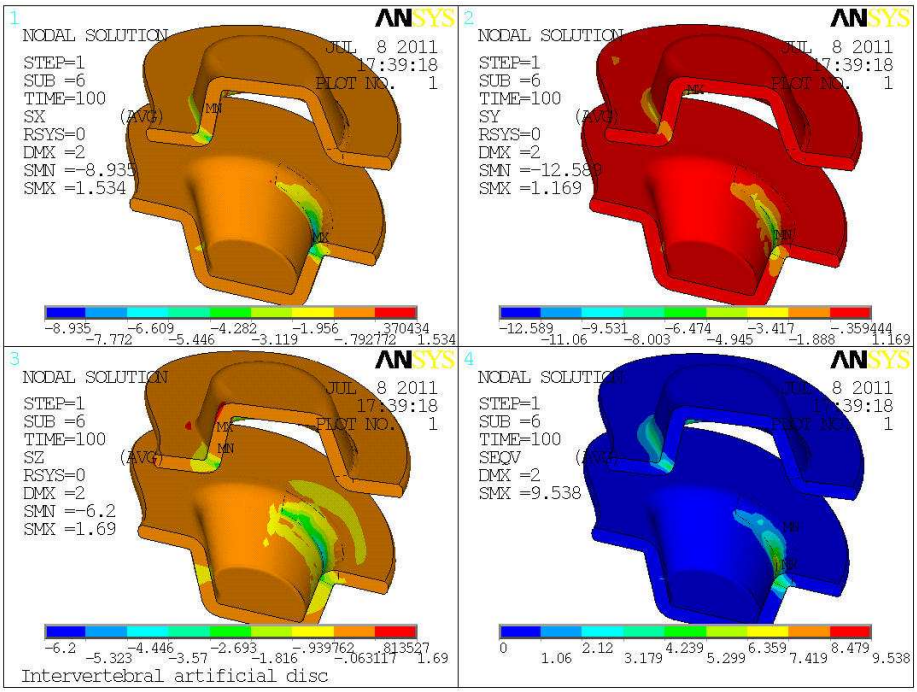

Figure 21: Sx, Sy, Sz and Seqv of the plate

In this case, greater compressive stresses are localized in the contacts between the metal plate and the hyperelastic inlay (*fig. 21 & 22*).

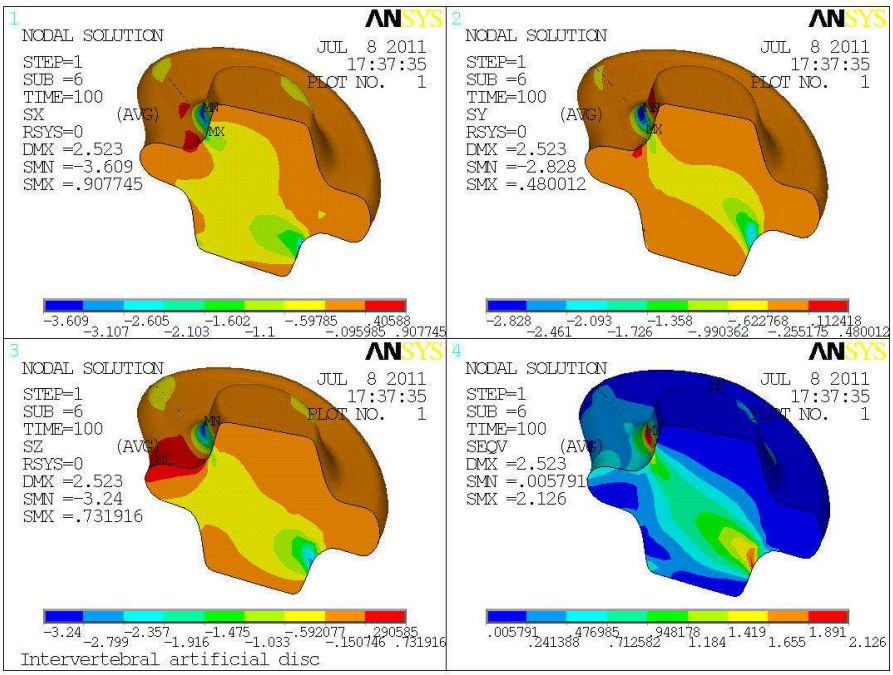

Figure 22: Sx, Sy, Sz and Seqv of the inlay

Because the analysis is performed with only one half of the intervertebral artificial disc, the reaction horizontal loads are not the real ones. In this case the real value of the horizontal

reaction in the X direction is the double of the one that ANSYS show. According to the previous comments, the intervertebral artificial disc under shear load has the following behavior:

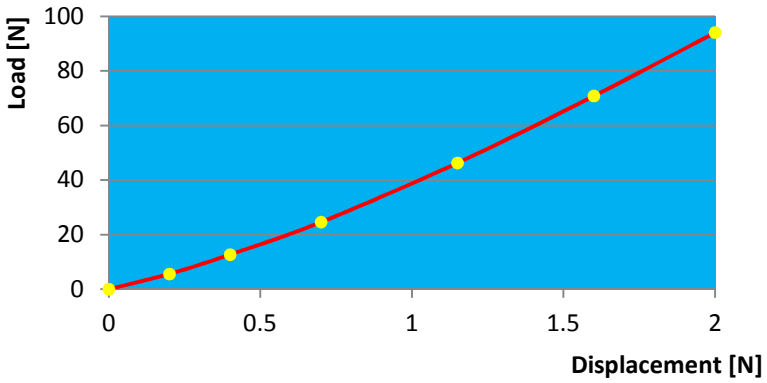

Figure 23: Shear force vs. displacement curve of the disc under shear load

Observing the graphic (*fig. 23*) it is possible to agree that under a shear load, the disc has a lineal response. As it was mentioned in the normal load analysis, these results do not match exactly with the real results because the real intervertebral disc is surrounded by other structures and tissues which absorb part of the applied loads.

Artificial disc analysis comments

ANSYS employs the "Newton-Raphson" approach (*fig. 24*) to solve nonlinear problems. In this approach, the load (in the previous analysis, the displacement) is subdivided into a series of load increments.

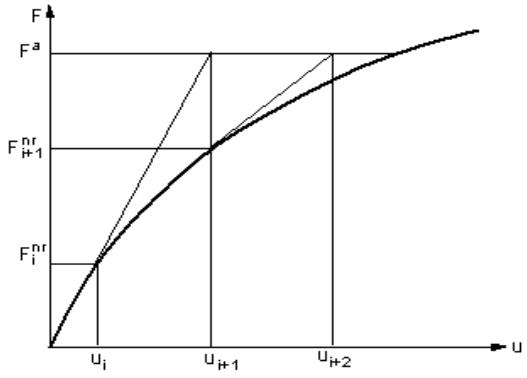

Figure 24: Diagram of the Newton-Raphson method [9]

The load increments can be applied over several sub steps. The artificial disc analysis were performed using a non constant load increment chosen by the program, it means that as the software is performing the solution it is choosing the time increment to achieve faster solution. In the first analysis where the load is applied vertically, the program needs several sets to achieve the solution, moreover in the second analysis, shear load, the program needed only six load steps. The next tables show the load sets with the displacement and reactions values. In the vertical load analysis, only the most significant values have been displayed due the high number of load sets.

Vertical load			Shear load		
Set	Displacement	Reaction	Set	Displacement	Reaction
0	0.00 mm	0.0000 N	0	0.00 mm	0.0000 N
1	0.40 mm	64.934 N	1	0.20 mm	5.5826 N
2	0.80 mm	132.94 N	2	0.40 mm	12.684 N
3	1.40 mm	309.78 N	3	0.70 mm	24.586 N
6	2.42 mm	900.64 N	4	1.15 mm	46.250 N
25	3.23 mm	3182.8 N	5	1.60 mm	70.804 N
264	4.00 mm	5848.2 N	6	2.00 mm	94.016 N

Table 1: Load sets with the displacement and their corresponding reaction.

Model of the lumbar spine

The next analysis is going to be performed using a model of the lumbar spine provided by Mr. Paweł Borkowski (*fig. 25*). First of all it is necessary to get the values of the parameters by measuring the spine model.

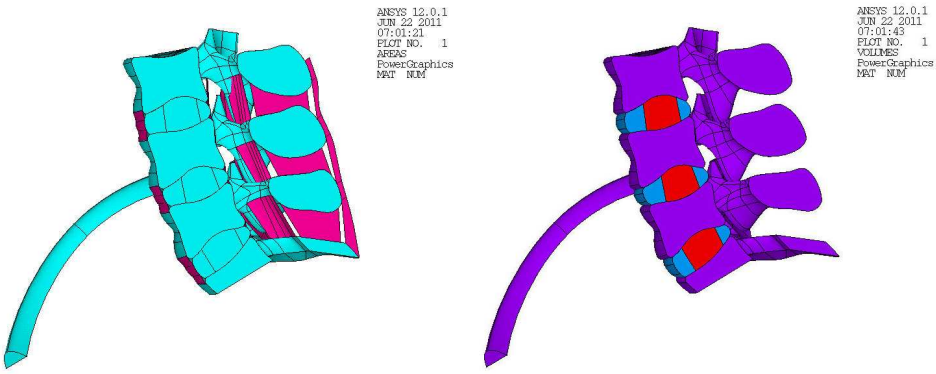

Figure 25: Images of the spine model: first one areas and second one volumes.

This model contains the most important structures of the spine. It is possible to differentiate the vertebrae (cortical and cancellous bone), the nucleus pulposus, the annulus fibrosus, part

of the pelvis and the ligaments that connect the vertebral bodies and the processes. The parameters used to build the intervertebral artificial disc (*fig. 26*) are the following ones:

S = 6.17 mm	G = 0 mm
alpha = 1.91˚	c = 11.69 mm
D = 30 mm	R_{int} = 1 mm
h = 7 mm	leap = 2 mm
L = 45 mm	slope = 1˚
P = 24.65 mm	R_{hyp} = 1 mm

Table 2: Values of the parameters of the prosthesis.

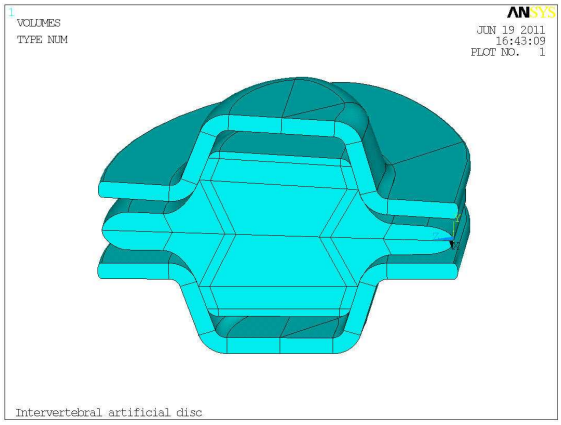

Figure 26: View of the artificial disc using the new parameters

The plate thickness is going to be considerate constant and its value is $t = 1.5\ mm$.

Assumptions for the analysis

To design and perform the analysis, some assumptions are going to be considered:

- The load state of the analysis is a vertical compression of the spine, like a static standing person.
- The anterior longitudinal ligament corresponding to the position of the L4-L5 disc is removed during the surgery.
- There is not any contact pair between the plates and the bone from the vertebrae, it is assumed the bone ingrowths into to the prosthesis.
- In the case where the prosthesis is not in its right position is because the implant has migrated to the anterior part of the spine.
- The iliac veins and arteries (*fig. 27*) are not affected by the disc migration; it is assumed that they are not broken or obstructed. This veins and arteries are the result of the bifurcation of the inferior cava vein and aorta artery.

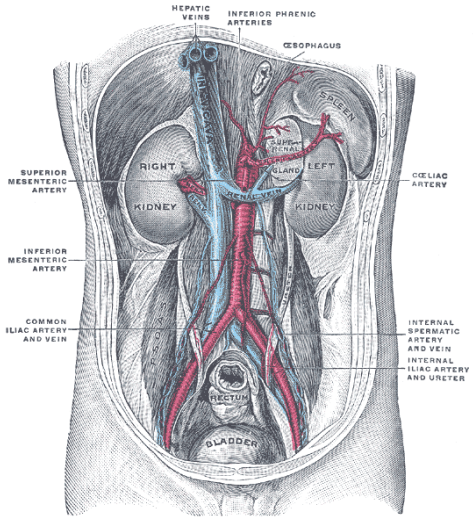

Figure 27: Principal blood vessels of the ventral zone of the human body [10]

- The surgery treatment is performed because the patient suffered from herniated disc, no vertebral bone has been affected of any fracture.
- It is assumed that the spine behavior is symmetric in the sagittal plane.
- When calculating moments it is assumed that the instant axis of rotation of the implant is normal to the sagittal plane and crosses the centre of the prosthesis.

Compression analysis of the lumbar spine with the artificial disc in its right position

To perform this analysis, the artificial disc is going to be situated in the middle of the intervertebral region, in its right position (*fig. 28*). In this case it is assumed that the surgeon has done his job well and he situated the disc in its right position. The aim of this analysis is to study the structural response of the lumbar spine on a given displacement and the disc behavior under the corresponding load. Our targets are going to be the displacements and stresses components on the bone and the implants and find the stiffness characteristics of the artificial disc. To apply this specific load, the nodes belonging to the upper area of the L3 are going to be forced to displace -1 mm in the vertical direction.

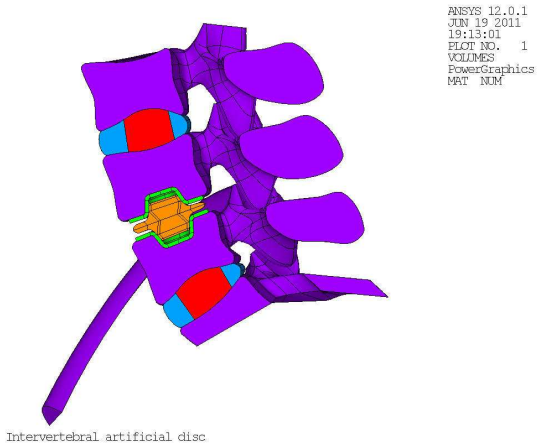

Figure 28: Lumbar spine with the disc in its right position

Actually in this analysis it is only interesting to study the adjacent structures of the artificial intervertebral disc (*fig. 29*) because they are the ones that are going to be modified during the surgery and actually their response is not known.

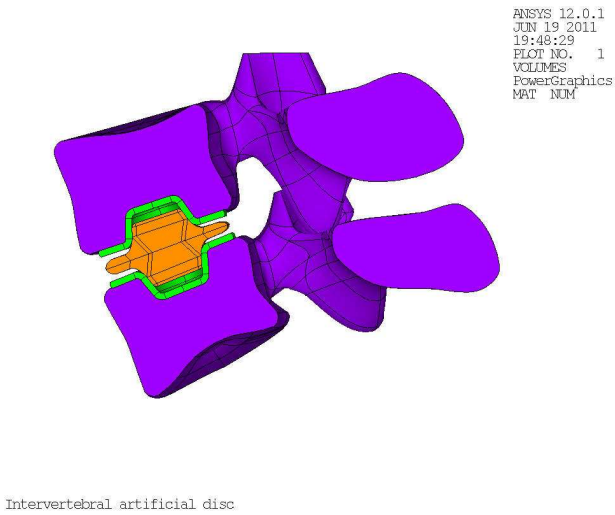

Figure 29: L4 and L5 with the artificial disc

The boundary conditions of this analysis are going to be similar to the ones of the artificial disc, it means all degrees of freedom constrained in the lower areas (the ones belonging to the S1 and the iliac crests), on the sagittal plane the areas (belonging to the vertebrae, the nucleus pulposus, the annulus fibrosus and the implant) are going to be constrained with symmetric boundary conditions and finally as it was mentioned before, the displacement of -1 mm in the vertical direction of the nodes belonging to the upper area of the L3. To ensure the stability on the lumbar spine model, one keypoint situated at the middle of the vertebral body of the L3 has been constrained in the horizontal direction. The solution method is going to be like the previous analysis performed with only the artificial disc.

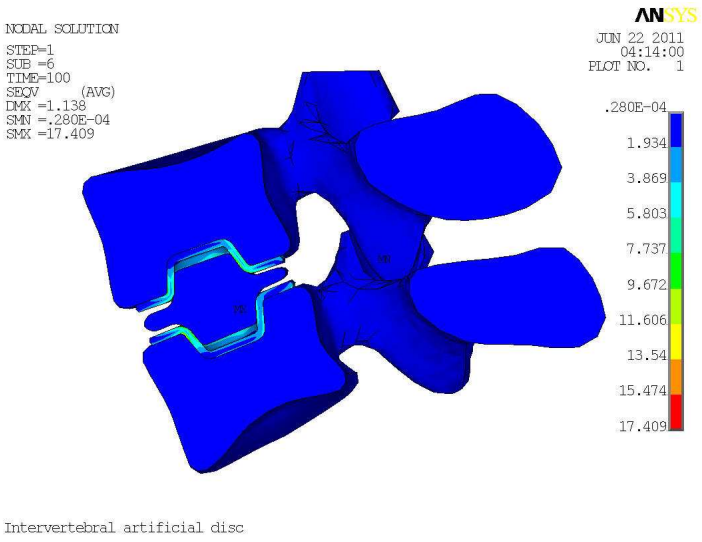

Figure 30: Equivalent stresses of the studied area

As can be observed in the previous figure (*fig. 30*), the places where greater efforts appear are the plates of the artificial intervertebral disc. If the stresses that appear in the plate are compared with the yield strength of the orthopedic alloys, they can be neglected.

But not only are the stresses of the implant important, the stresses that are found in the bone are also important. Compared with the prosthesis, the bone is much weaker. It is important to know where the stresses are focalized and which their value is. Both kinds of bones, cortical and cancellous, must be studied.

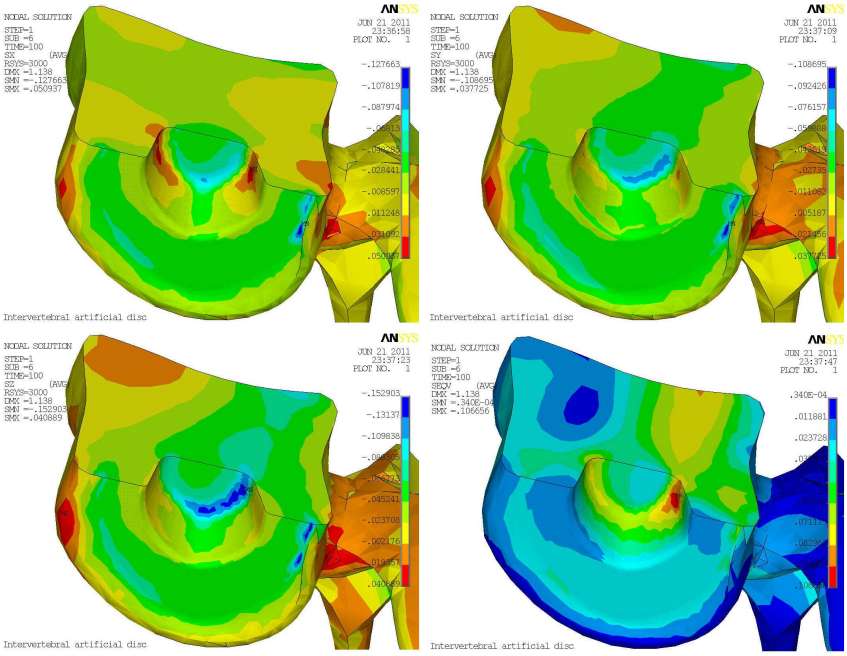

Figure 31: Sx, Sy, Sz and Seqv of the cancellous bone from the vertebral bone.

The stresses of the pervious images (*fig. 31*) have been displayed using the vertebrae coordinate system, where the positive XY plane coincides with the socket plane of the bone and the X direction is on the anterior-posterior line. According to the previous images, greater stresses are localized in the internal edge of the bone socket but they are not high enough to damage the bone.

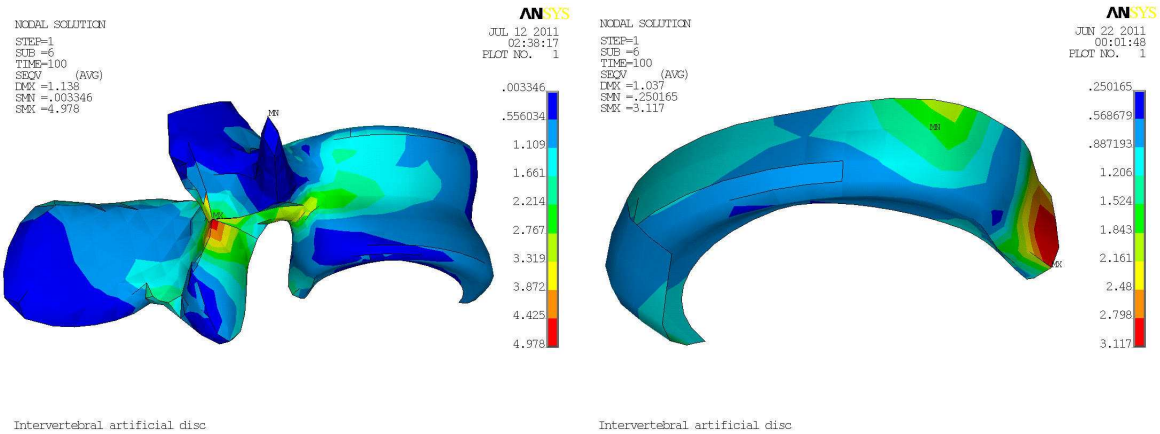

Figure 32: Von Mises stresses of the cortical bone from the lower vertebral body.

Comparing the stresses of the cancellous bone with the ones from the cortical bone, it is remarkable that the cortical ones are significantly higher than the firsts (*fig. 32*). In the cortical bone, the concentration of stresses is found in the posterior part of the vertebral body, in the place where the posterior longitudinal ligament is found. Some stresses concentrations can be

observed in the lower part of the vertebral body, in the areas in contact with the plate, this stress concentrations appear because of the element concentrations, so they don't show the real state of stresses.

The behavior of the disc under the compressive load can be displayed as the relation between the load in the middle plane of the implant and the distance between the plates. Because the analysis is being performed using the half of the lumbar spine, the load results are the half of the real ones.

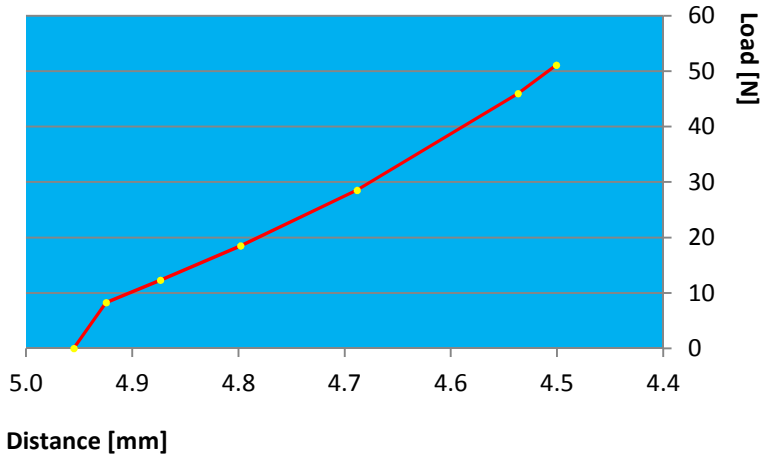

Figure 33: Normal force vs. distance curve of the prosthesis under a vertical load

The previous graphic (*fig. 33*) shows the response of the artificial disc assembled with the lumbar spine model. As expected the load increases as the metal plates get closer. The total relative displacement between the metal plates at the end of the load is 0.454 mm. It is remarkable that when the load is applied there is a fast increment of the load on the disc and then the load increases substantially straight.

Distance [mm]	Displacement [mm]	Normal force [N]
4.96	0.0000	0.000
4.92	0.0304	8.276
4.87	0.0815	12.301
4.80	0.1571	18.505
4.69	0.2667	28.507
4.54	0.4184	45.960
4.50	0.4544	51.071

Table3: Distance, displacement and normal force over the midplane of the inlay

In this case, is also interesting to study the shear stresses that appear at the midplane of the inlay (*fig. 34)*.

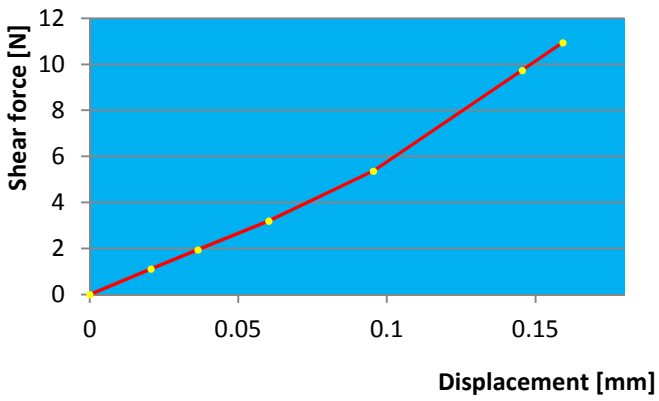

Figure 34: Shear force vs. displacement of the prosthesis under a vertical load

As it can be observed in the previous figure, the shear force over the midplane of the inlay does not have the same behavior as the normal force.

Displacement [mm]	Shear force [N]
0.0000 mm	0.000 N
0.0206 mm	1.116 N
0.0364 mm	1.941 N
0.0602 mm	3.196 N
0.0954 mm	5.362 N
0.1455 mm	9.737 N
0.1591 mm	10.94 N

Table 4: Displacement and shear force over the midplane of the inlay

The moment that appears in the prosthesis is also interesting to study the behavior of the artificial intervertebral disc (*fig. 35*).

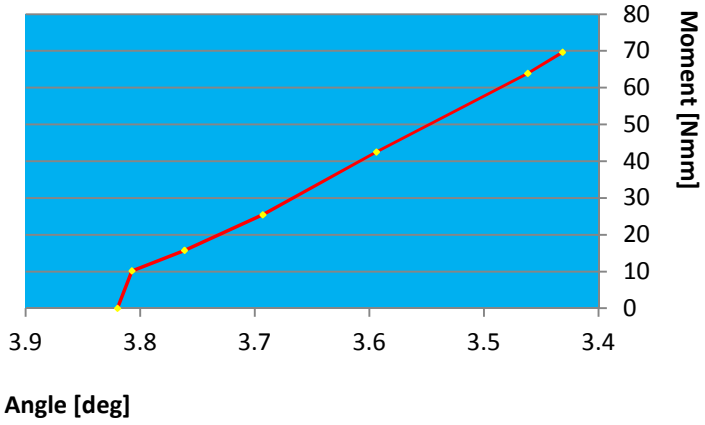

Figure 35: Moment vs. angle curve of the prosthesis under a vertical load

As happened in the normal force curve, at the beginning of the load there is a fast increment of moment.

Angle [deg]	Rotation [deg]	Moment [Nmm]
3.82	0.0000	0.000
3.81	0.0126	10.171
3.76	0.0585	15.742
3.69	0.1269	25.434
3.59	0.2261	42.543
3.46	0.3582	63.890
3.43	0.3886	69.640

Table 5: Angle, rotation and moment over the midplane of the inlay

Compression analysis of the lumbar spine with the artificial disc in its bad position

To perform the analysis of the artificial intervertebral disc in its bad position, the prosthesis is going to be moved towards the anterior direction of the vertebra (*fig. 36*).

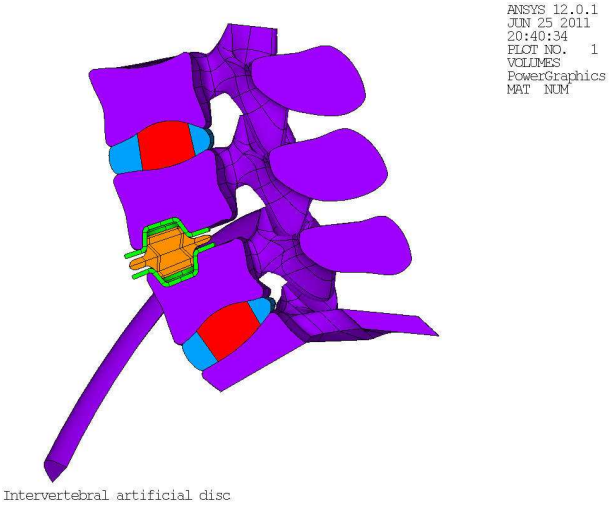

Figure 36: Lumbar spine with the disc in its bad position

As in the previous analysis, the structures which are interesting to study are the vertebrae adjacent to the artificial intervertebral disc (*fig. 37*).

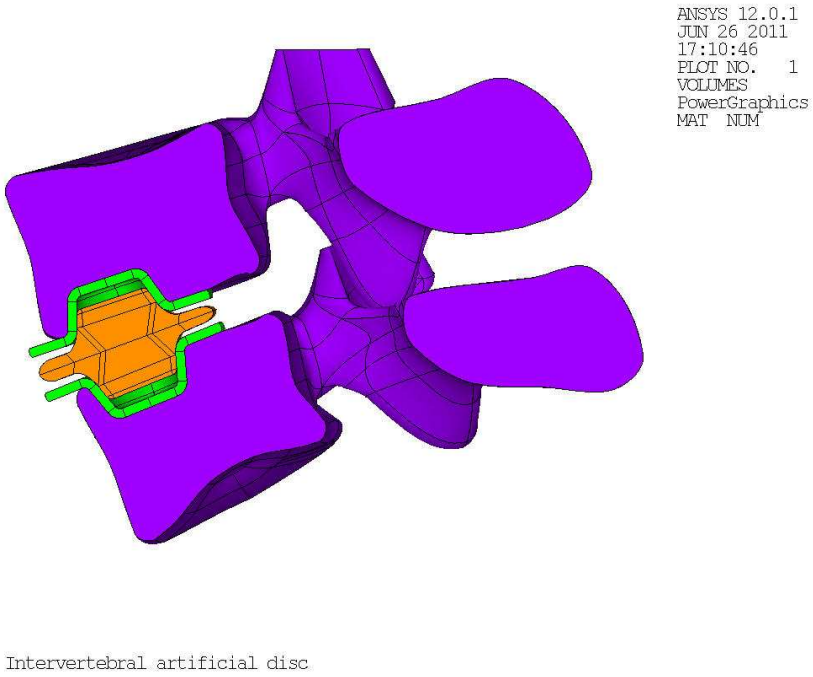

Figure 37: L4 and L5 with the disc in its wrong position

To compare the behavior of the artificial intervertebral disc the conditions of the analysis must be the same in both situations. All degrees of freedom of the lower areas (S1 and iliac crests) are going to be constrained, on the sagittal plane the areas (vertebrae, nucleus pulposus,

annulus fibrosus and the implant) are going to be constrained with symmetric boundary conditions and finally the displacement of -1 mm in the Y direction of the nodes belonging to the upper area of the L3. As in the previous analysis, to ensure the stability on the lumbar spine model, one keypoint situated at the middle of the vertebral body of the L3 has been constrained in the horizontal direction. The solution method is going to be like the previous analysis performed with the artificial disc in its right position.

As it can be seen in the next image (*fig. 38*), where the equivalent stresses of the studied area are showed, the higher values are found in the metal plates of the implant. The stresses that appear at the metal plates are not problematic because if they are compared with the yield stress of the orthopedic alloys, they can be neglected.

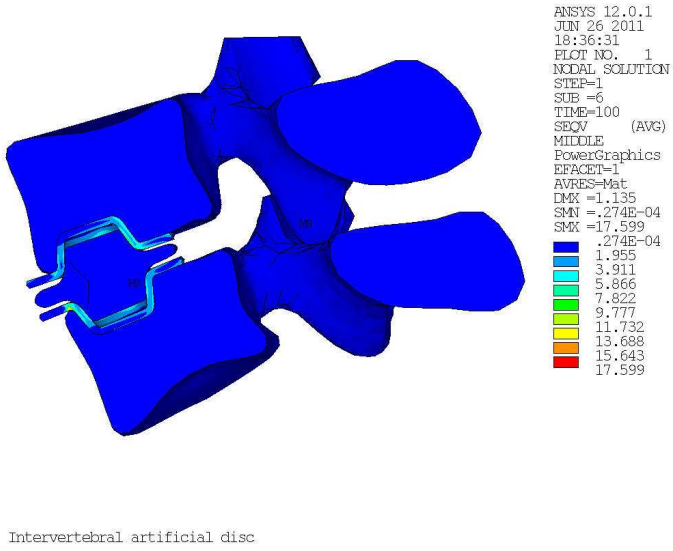

Figure 38: Von Mises stresses of the studied area

In this analysis is very important to study the response of the vertebral bone. With the disc in its bad position, there is a thin wall of bone in the anterior part of the vertebral body that could be damaged if the stresses are high enough.

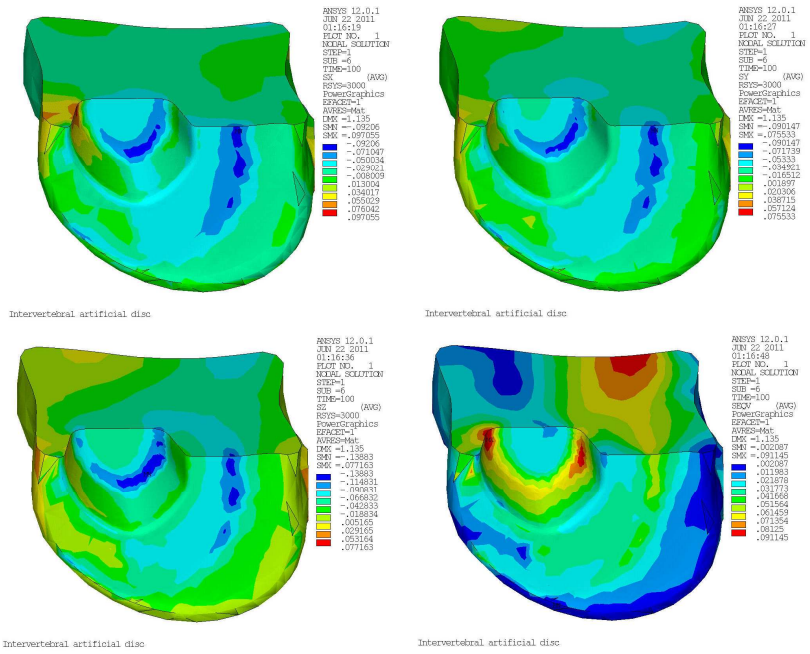

Figure 39: Sx, Sy, Sz and Seqv of the cancellous bone from the vertebral bone.

The stresses of the pervious images (*fig. 39*) have been displayed using the vertebrae coordinate system, where the positive XY plane coincides with the socket plane of the bone and the X direction is on the anterior-posterior line. According to the previous images, and as it was supposed, there is a stress concentration on the thin wall of bone situated at the anterior part of the vertebral body that at the analysis of the implant in its right position did not appear. At first, it seems that the stresses that are found in the thin bone wall are not enough to damage the bone, but if the spinal load increases the stresses could increase until the bone rupture limit and damage it.

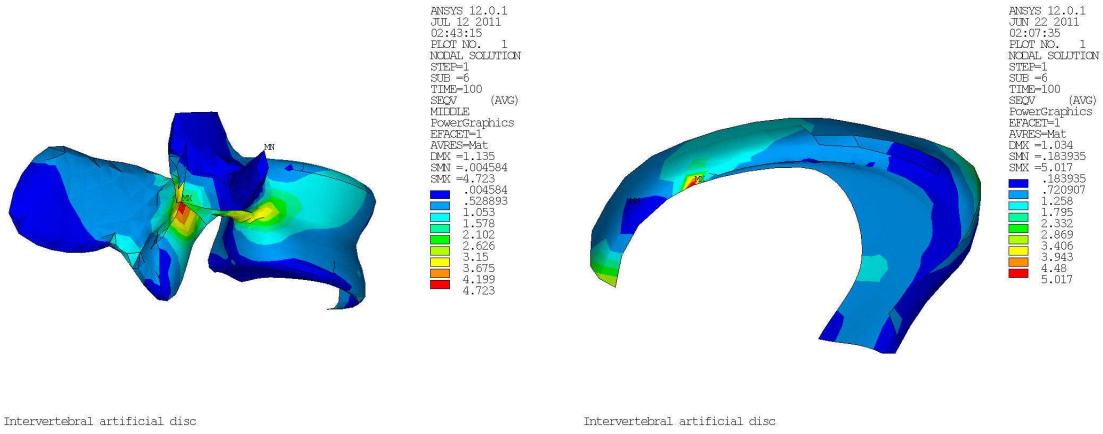

Figure 40: Von Mises of the cortical bone from the lower vertebral body.

Comparing the stresses of the cancellous bone with the ones from the cortical bone (*fig. 40*), it is remarkable that the cortical ones are significantly higher than the firsts. In the cortical bone, the concentration of stresses is found in the anterior part of the vertebral body, in the place where the plate gets in touch with the bone. Some local concentrations can be observed in the lower part of the vertebral body, there is a tress concentration in the anterior part of the cortical bone and where the plates get in touch with the bone.

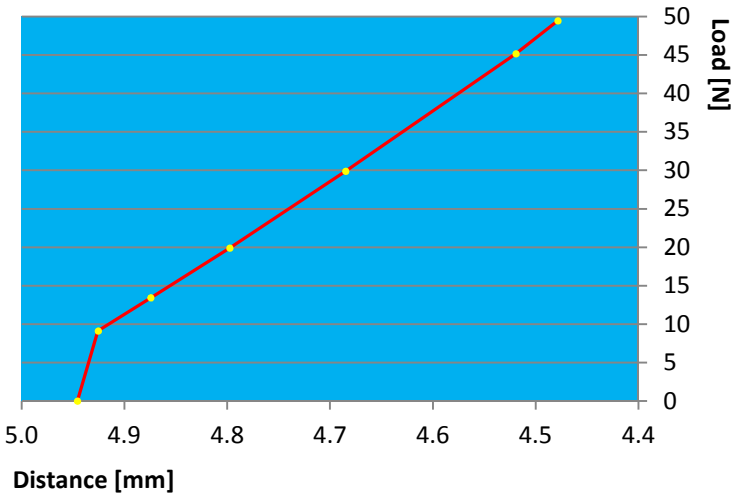

Figure 41: Normal force vs. distance curve of the prosthesis under a vertical load

The previous graphic (*fig. 41*), shows the response of the artificial disc assembled with the lumbar spine model. As expected the load increases as the metal plates get closer. The total relative displacement between the metal plates at the end of the load is 0.467 mm. It is remarkable that when the load is applied there is a fast increment of the load on the disc and then the load increases substantially straight.

Distance [mm]	Displacement [mm]	Normal force [N]
4.95	0.0000	0.000
4.93	0.0201	9.113
4.87	0.0713	13.436
4.50	0.1481	19.899
4.68	0.2609	29.887
4.52	0.4264	45.157
4.48	0.4672	49.437

Table 6: Distance, displacement and normal force over the midplane of the inlay

It is also interesting to observe the relation between the shear load and the horizontal relative displacement between the metal plates.

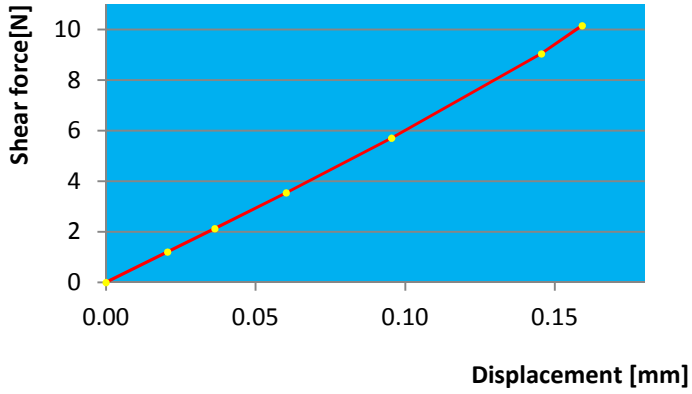

Figure 42: Shear force vs. displacement curve of the prosthesis under vertical load

As it can be observed in the previous figure (*fig. 42*), shear force over the midplane of the inlay do not has the same behavior as the normal force, shear force has a substantially linear behavior.

Displacement [mm]	Shear force [N]
0.0000 mm	0.000 N
0.0206 mm	1.207 N
0.0364 mm	2.128 N
0.0602 mm	3.545 N
0.0954 mm	5.707 N
0.1455 mm	9.039 N
0.1591 mm	10.153 N

Table 7: Displacement and shear force over the midplane of the inlay

The behavior is also studied using the moments that appears in the disc.

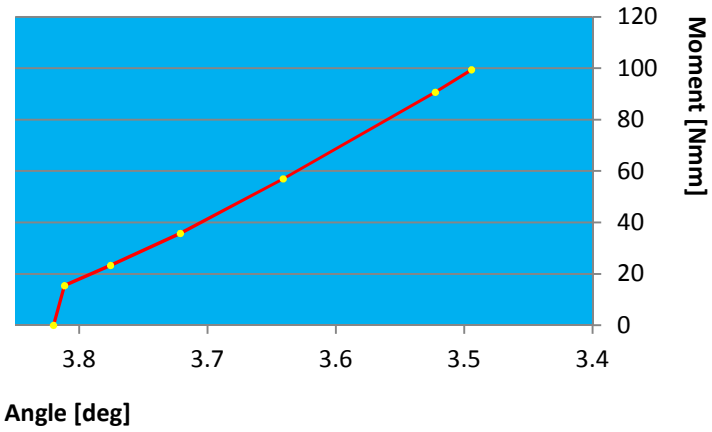

Figure 43: Moment vs. angle curve of the prosthesis under a vertical load

As happened in the load curve, there is a first fast increment of the moment and then the curve increases substantially straight (*fig. 43*).

Angle [deg]	Rotation [deg]	Moment [Nmm]
3.82	0.0000	0.000
3.81	0.0086	15.422
3.78	0.0444	23.310
3.72	0.0988	35.734
3.64	0.1789	56.995
3.52	0.2974	90.643
3.49	0.3256	99.423

Table 8: Angle, rotation and moment over the midplane of the inlay

Comparison of the compressive analysis

Comparing both analysis, there are some results that may be surprising. The first results that are interesting are the maximum stresses of the vertebrae.

	Right position [N/mm^2]	Bad position [N/mm^2]
Sx	0.127663 (c)	0.090147 (c)
Sy	0.037725 (c)	0.148475 (c)
Sz	0.040889 (c)	0.099146 (c)
Seqv	0.106656	0.091145

Table 9: Maximum stress values over the trabecular bone of the vertebra

As it could be supposed, in the analysis where the disc is not placed in its right place, the stresses are greater than the ones from the analysis where the disc is placed in its right position. In the other hand it is remarkable that the maxim Von Mises stress in the first analysis is nearly the same as in the second one.

Another fact that must be commented is the situation of the higher values of the stress. In the first analysis the higher tensile values of Sx and Sy are found in the bone socket and in the junction of the vertebral body with the pedicle, on the other hand, the higher compressive values of Sx are found in the contact between the vertebral body and the posterior part of the metal plate. About the Sz stresses, maximum tensile values, are found in the junction of the vertebral body with the pedicle, on the other hand, maximum compressive values are found in the bone socket and in the posterior part of the vertebral body .In the first case, the maximum equivalent stress of the first analysis is found in the junction of the vertebral body with the pedicle.

However, all maximum compressive stresses, Sx, Sy and Sz, of the second analysis are found in the bone socket and in the contact of the upper metal plates of the implant and the posterior

part of the vertebral body. In the other hand, maximum tensile stress values are found in the junction of the vertebral body with the pedicles. In this case, the maxim equivalent stress is found in the socket of the vertebral body (*figure 44*).

In any case, these stresses are enough to damage the trabecular bone because its ultimate stress is about 8 MPa[6], but if the load increases, probably these stresses will increase until its critical values and damage the bone structures.

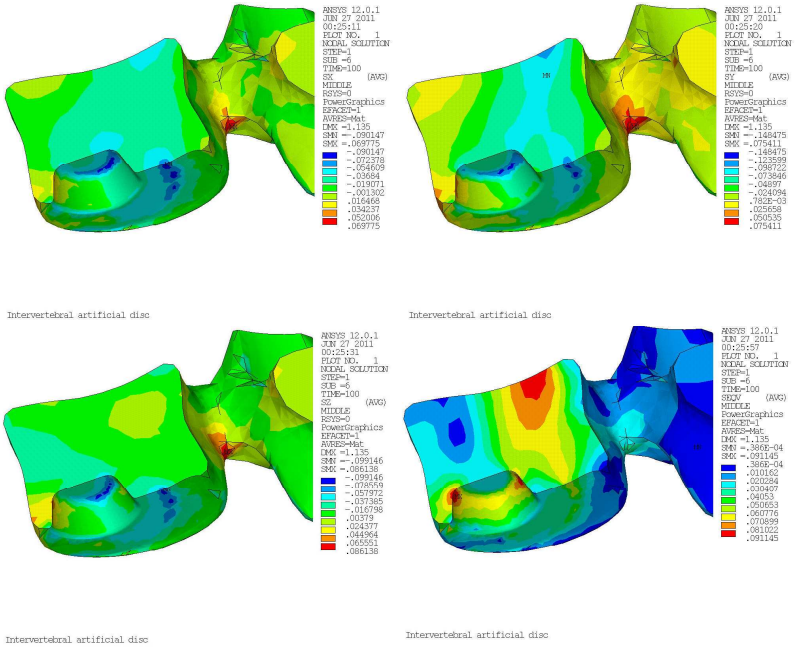

Figure 44: Sx, Sy, Sz and Seqv of the cancellous bone from the vertebral bone.

Higher equivalent stresses of the cortical bone are found in the vertebral lamina. If the equivalent stresses of the cortical bone of the lower vertebral body are compared from one analysis to the other (*fig. 45*), ignoring the local concentration due to the element accumulation, it can be observed that in the first case, higher values of stress are found in the posterior part of the vertebral body whereas in the second case are found in the anterior part of the vertebral body. In both cases, according to the next images, the maximum Von Mises stresses have similar values. As happened to the previous comments of the trabecular bone, currently stresses are not enough to damage the bone because its ultimate stress is about 100 MPa[7]

[6] NORDIN, M.; FRANKEL, V.H. (2001). *Basic Biomechanics of the Musculoskeletal System.* 3rd ed. Lippincott Williams & Wilkins. ISBN: 0-683-30247-7

[7] NORDIN, M.; FRANKEL, V.H. (2001). *Basic Biomechanics of the Musculoskeletal System.* 3rd ed. Lippincott Williams & Wilkins. ISBN: 0-683-30247-7

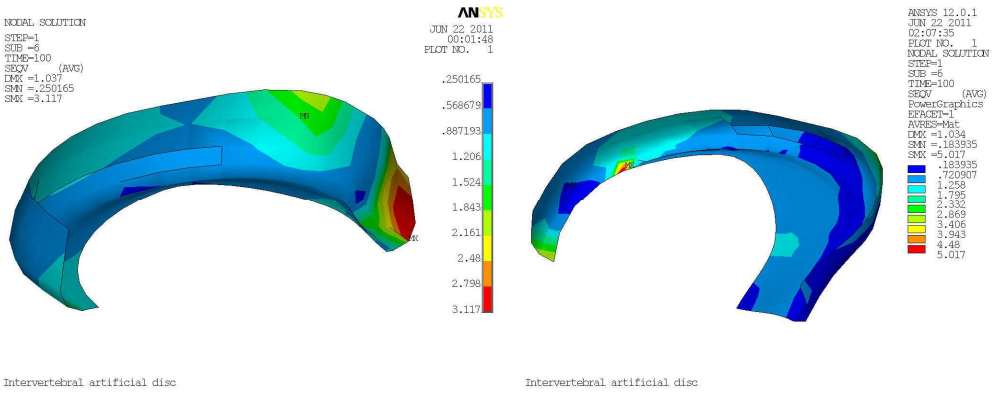

Figure 45: Von Mises stresses of the cortical bone in both disc positions.

Although it seems that it doesn't have to be, the artificial disc has a similar behavior in both analyses. If the load and moment curves of the two cases are compared it is clearly that they have the same shape (*fig. 46*), but the substantial difference between their behaviors is that the moment (*fig. 48*) over the artificial disc in its bad position is between a 30 and a 50% greater than the moment of the disc in its right position.

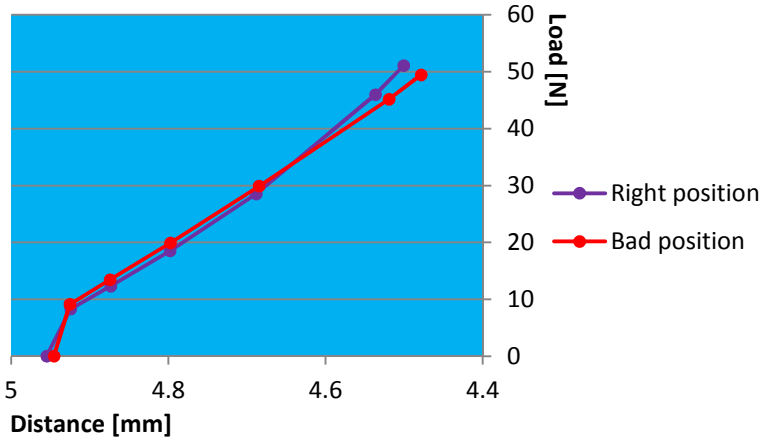

Figure 46: Normal force vs. distance curve of both analyses

There is the need to remember that these analysis are performed with only one half of the spine which means that the loads and the moments that are shown on the graphics are the ones from the model, and to extrapolate these values to the real spine they have to be doubled.

The initial fast increment of load that appears in the normal load curve is probably because of the movement of the prosthesis. At the beginning of the load, the interior plate edges contact with the inlay highly compressing it and after this the movement of the adjacent vertebrae

move the plates in such way that the inlay gets normally compressed getting the new slope of the curve.

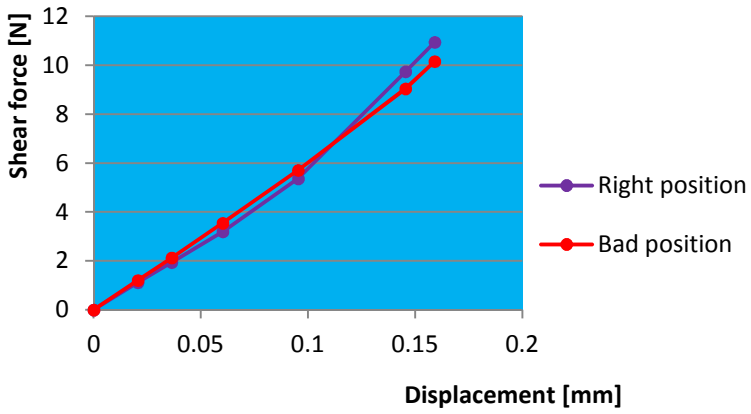

Figure 47: Shear force vs. distance curve of both analyses

As happens with the normal force, shear force in both analyses has a substantially similar behavior (*fig.47*).

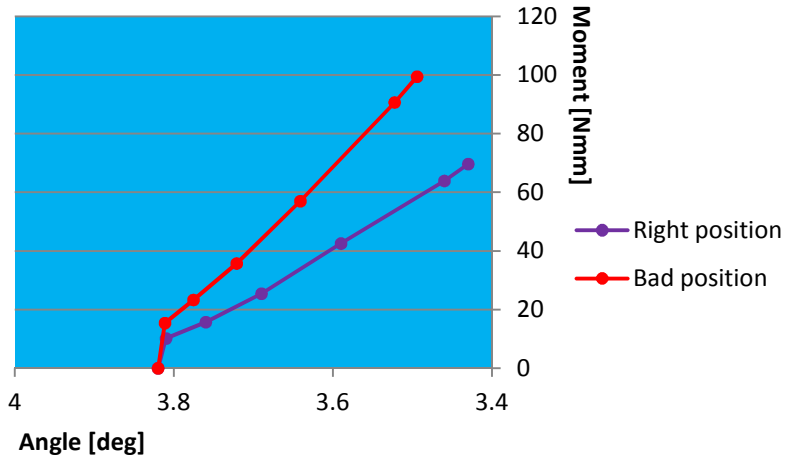

Figure 48: Moment vs. angle curve of both analyses

Could be normal that the artificial disc which is not in its right position experiments a higher moment (*fig.48*). In this case, the adjacent vertebrae act like a tweezers where the processes act as the fulcrum of this 3rd class lever.

As it is knew, the real intervertebral disc has the behavior of a hyperelastic material, and the artificial intervertebral disc has to, but it can be seen in the normal force vs. distance graphic (*fig. 44*) of the intervertebral artificial disc has not the behavior of a hyperelastic material. As

can be found in the literature[8], the slope of the strain-stress curve of an intervertebral disc is about 800 N/mm until a load of 1 kN, after that load the slope increases to 2000 N/mm. The reason why the implant has this bad behavior is due to the gap between the metal plate brims and the inlay.

Combined analysis of the lumbar spine with the artificial disc in its right position

This analysis is going to be a combined analysis where a vertical and a horizontal displacement are going to be applied. When the horizontal effort increases considerably, the structures of the spine can be damaged producing the known spondylolisthesis. The aim of this analysis is to study the lumbar and the intervertebral artificial disc response. Under a horizontal effort, the inlay of the artificial disc could be placed in a bad position because of the prosthesis design. To create the combined load we are going to make some calculations.

The displacement applied to the upper areas of the L3 is going to have the same direction as the midplane of the prosthesis inlay. To propose the solution to this problem a temporal coordinate system (*fig. 49*) this has the same axis of the general coordinate system of the model of the lumbar spine but with different names.

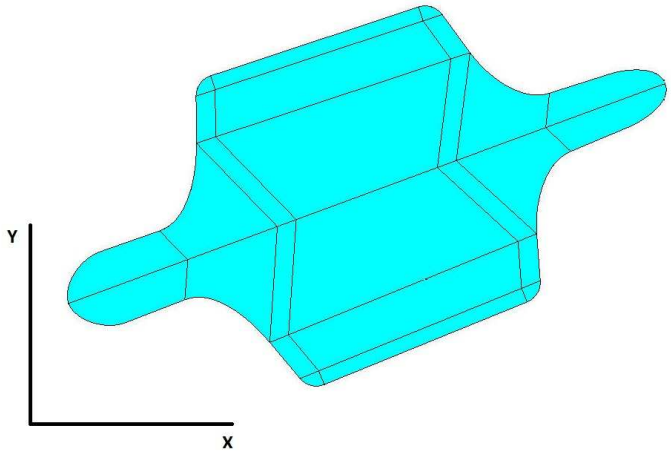

Figure 49: Sagittal view of the inlay with the temporal coordinate system.

It is assumed that the line the line defined by the mid plane of the inlay and the symmetry plane of the lumbar spine can be defined by the equation $y = m \cdot x + n$, where m is the slope of the line and n is the ordinate at the origin. If a down displacement d_y is applied to this line,

[8] Eijkelkamp M. F., van Donkelaar C. C., Veldhuizen A. G., van Horn J. R., Huyghe J. M.: *Requirements for an artificial intervertebral disc*, The International Journal of Artificial Organs 24:311-321, 2001.

its new equation will be $y = m \cdot x + n - d_y$. Now, a new displacement d_x is applied, and the aim is that the resulting line stays at the same place as the first line. The resulting equation after the d_x displacement will be $y = m \cdot (x + d_x) + n - d_y$. According to the previous comments, the first equation must be equal to the second one. In both equations are equaled, we find that $d_y = m \cdot d_x$. As it is known, the slope of a linear function is the tangent of the angle between the linear function and the X axis. First of all, to apply the displacement, it is needed to know this angle; in this case this angle is about 19.557˚. In this analysis we are going to apply a horizontal displacement of 5 mm therefore the vertical displacement will be, according to the previous comments:

$$d_y = m \cdot d_x = \tan(19.557°) \cdot 5 = 1.776 \text{ mm}$$

The boundary conditions applied to the next analysis are going to be the same as the previous ones but with the difference that there is no keypoint restricted in the sagittal plane to stabilize the lumbar spine.

This analysis will be useful to study the stresses that appear in the junction of the vertebral body with the pedicles produced by the instability of the inlay of the intervertebral device.

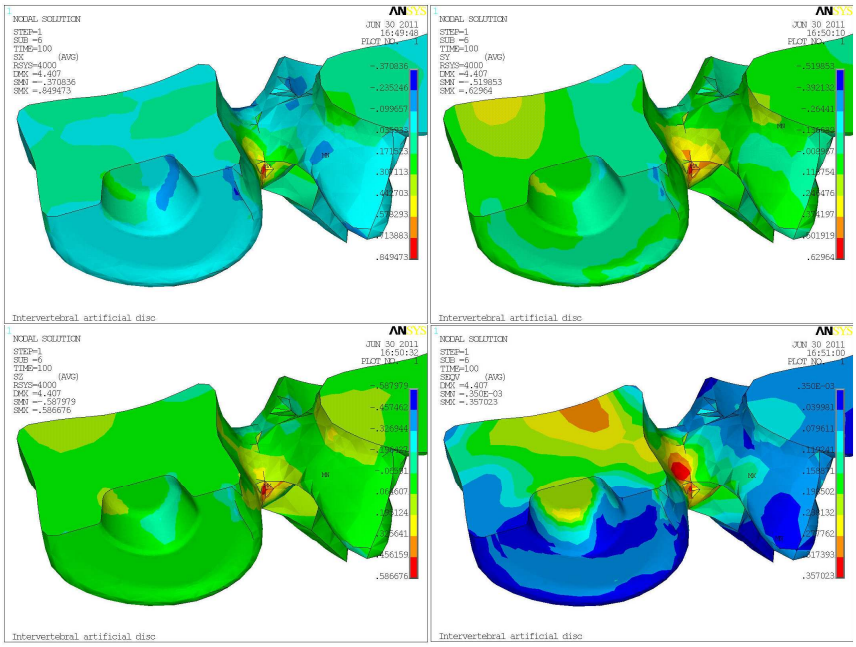

Figure 50: Sx, Sy, Sz and Seqv of the cancellous bone from the vertebral bone.

In this case (*fig. 50*) is more evident that the most stressed part of the vertebra is the junction of the vertebral body with the pedicles, which is obvious considering the type of the applied load.

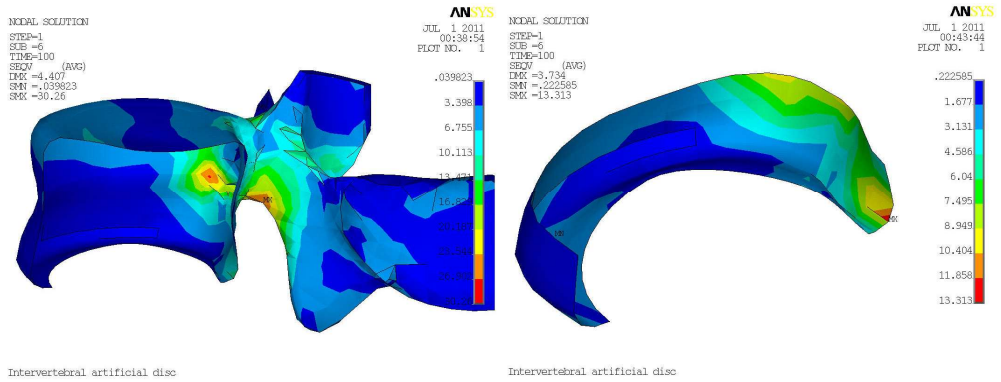

Figure 51: Von Mises stresses of the cortical bone with detail of the lower vertebral body.

The maximum equivalent stress in the cortical bone (*fig. 51*) is located in the same place as the maximum Von Mises stresses of the trabecular bone; in this case, the stress values are considerably high, rising a maximum value of 30.26 MPa. If the lower cortical bone of the vertebral body is observed, higher values of the equivalent stresses are found in the posterior part of the vertebral body, this maximum equivalent stress of the lower cortical bone is about 13.31 MPa.

Under this load state, the stresses of the vertebrae are starting to be considerable but comparing with the ultimate stress of both types of bone are not enough to damage any structure.

As it was mentioned previously, under the combined load, the inlay enters into a bad position producing the malfunction of the prosthesis (*fig.52*).

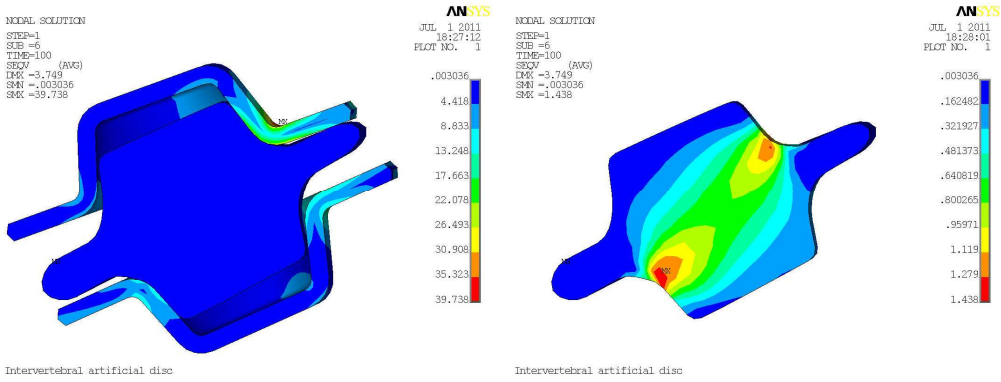

Figure 52: Inlay into its bad position with its Von Mises stresses.

In this analysis, a part of showing the compressive and moment response of the inlay, the shear load experienced by the inlay of the intervertebral disc it is also going to be displayed.

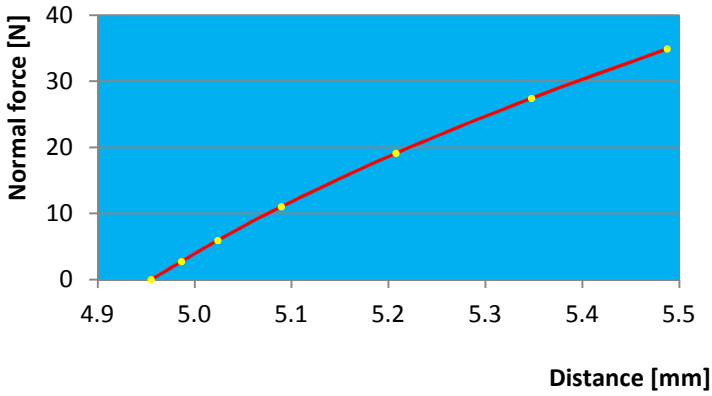

Figure 53: Normal force vs. distance curve of the prosthesis under a combined load

Distance [mm]	Displacement [mm]	Normal force [N]
4.96	0.0000	0.000
4.99	-0.0313	2.737
5.02	-0.0687	5.933
5.09	-0.1343	11.043
5.21	-0.2525	19.118
5.35	-0.3924	27.434
5.49	-0.5324	34.912

Table 10: Distance, displacement and normal force over the midplane of the inlay

In this case the compressive loads (*fig. 53*) are lower than the ones of compression analysis of the spine although the applied vertical displacement in this case is greater. This is because if an anterior displacement is applied, the distance between the vertebrae increases thus preventing the compression of the inlay. As it could be observed in the previous graphic, the load increases while the distance between the plates increases with a nearly constant slope.

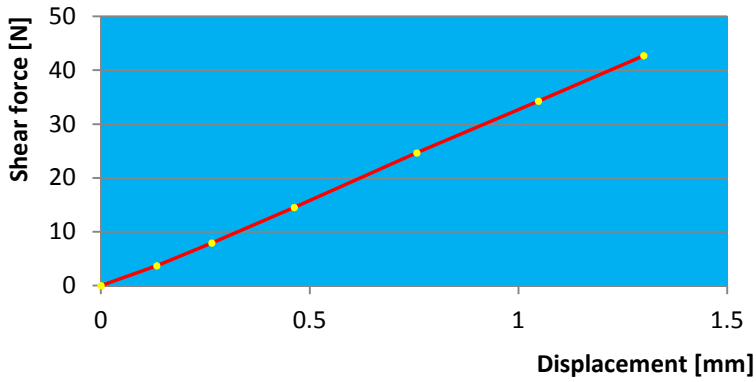

Figure 54: Shear force vs. displacement curve of the prosthesis under a combined load

Displacement [mm]	Shear force [N]
0.0000	0.000
0.1337	3.685
0.2655	7.921
0.4628	14.509
0.7567	24.659
1.0480	34.275
1.3000	42.723

Table 11: Displacement and shear force over the midplane of the inlay

In the shear force vs. displacement curve (*fig. 54*), the displacement has been calculated as the relative displacement between the metal plates of the artificial disc. As in the control analysis under shear load of the artificial intervertebral disc the shear curve has the same lineal behavior but not the same slope, this could be because in this case the midplane of the inlay and the plate plain don't preserve the same orientation during the analysis.

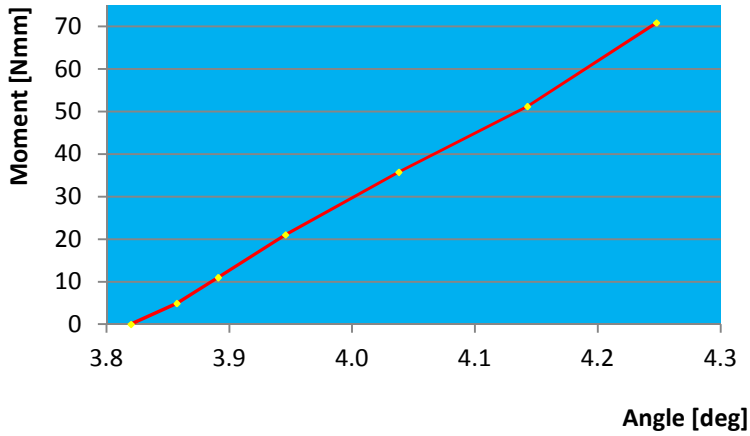

Figure 55: Moment vs. angle curve of the prosthesis under a combined load

Angle [deg]	Rotation [deg]	Moment [Nmm]
3.82	0.0000	0.000
3.86	0.0373	4.895
3.89	0.0710	10.987
3.95	0.1258	21.001
4.04	0.2180	35.735
4.14	0.3227	51.174
4.25	0.4277	70.834

Table 12: Angle, rotation and moment over the midplane of the disc

As happened in the normal force curve where the distance between the metal plates increases with the normal force (*fig. 53*), in the moment curve (*fig. 55*) the angle increases while the moment increases too.

Combined analysis of the lumbar spine with the artificial disc in its bad position

In this case, the angle of the inlay of the artificial disc and the anterior direction is about 21.38˚ and according to the previous calculations if a horizontal displacement of 5 mm is applied then the vertical displacement must be about 1.958 mm. The boundary conditions of this analysis are going to be the same ones as the previous combined load analysis.

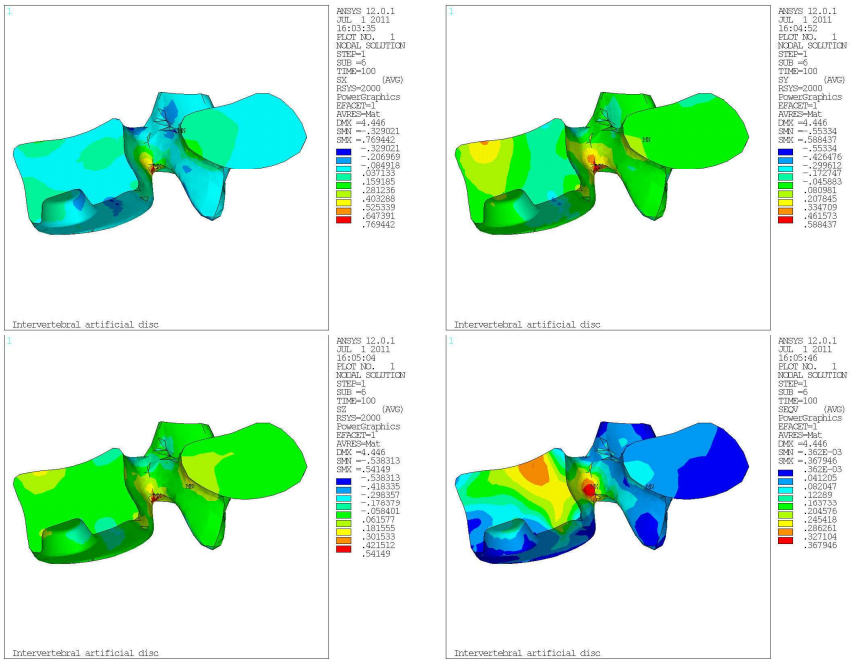

Figure 56: Sx, Sy, Sz and Seqv of the cancellous bone from the vertebral bone.

The maximum compressive Sx and Sy (*fig. 56*) are located in the lower part of the vertebral body, moreover, the maximum tensile Sx and Sy stresses are located in the pedicle of the vertebral arch. About the Sz stresses, the maximum compressive stress is found in the pars interarticularis and the maximum tensile stress is placed in the junction of the vertebral body with the pedicle, as happen with the maximum Seqv stress.

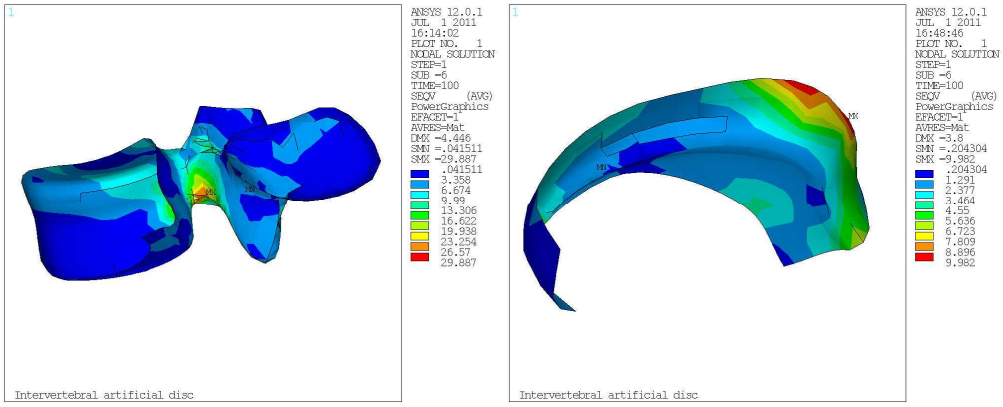

Figure 57: Von Mises stresses of the cortical bone with detail of the lower vertebral body.

In the previous images (*fig. 57*) the Von Mises stresses of the cortical bone are showed. As it was anticipated, maximum stress is found in the junction of the vertebral body with the pedicle with a maximum value of 29.877 MPa. If the lower cortical bone of the vertebral body is observed, the maximum equivalent stresses are found in the lateral posterior part of the vertebral body, this maximum Von Mises stress has a value of 9.892 MPa, which is directly related with the maximum stress located in the vertebral body junction with the pedicle.

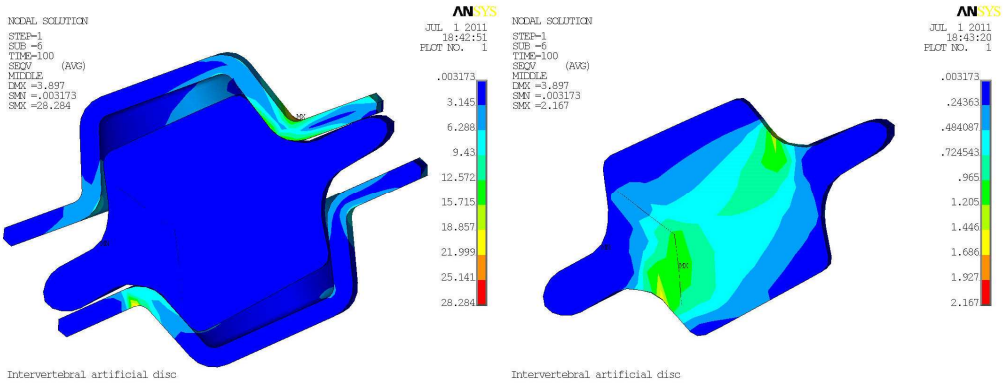

Figure 58: Inlay into its bad position with its Von Misses stresses.

In this case, the hyperelastic inlay places itself into a bad position thus causing a non-optimal operation of the implant (*fig. 58*). As expected, higher values of equivalent stress are found in the contact points between the inlay and the metal plates.

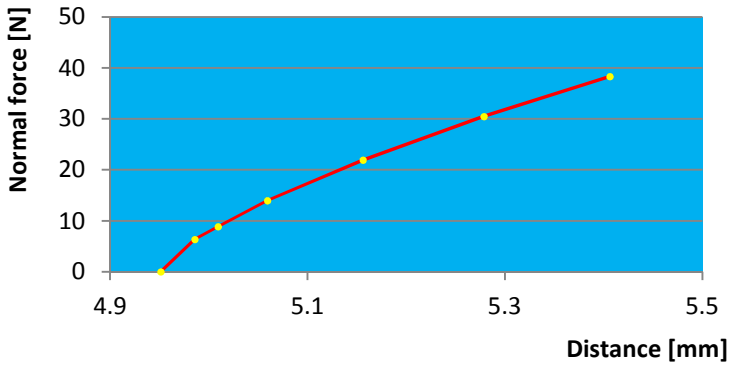

Figure 59: Normal force vs. distance curve of the prosthesis under a combined load

Distance [mm]	Displacement [mm]	Normal force [N]
4.95	0.0000	0.000
4.99	-0.0345	6.373
5.01	-0.0580	8.862
5.06	-0.1080	13.975
5.16	-0.2048	21.939
5.28	-0.3273	30.485
5.41	-0.4548	38.306

Table 13: Distance, displacement and normal force over the midplane of the inlay

As happened in the previous analysis, while the distance between the metal plates increases, the normal force experienced by the inlay increases too (*fig. 59*). This unexpected behavior happens because as the vertical distance between the metal plates increases, the relative horizontal displacement of the metal plates increases also. At this point, the shear effort produced by the relative horizontal displacement of the plates creates a normal force to the midplane of the inlay.

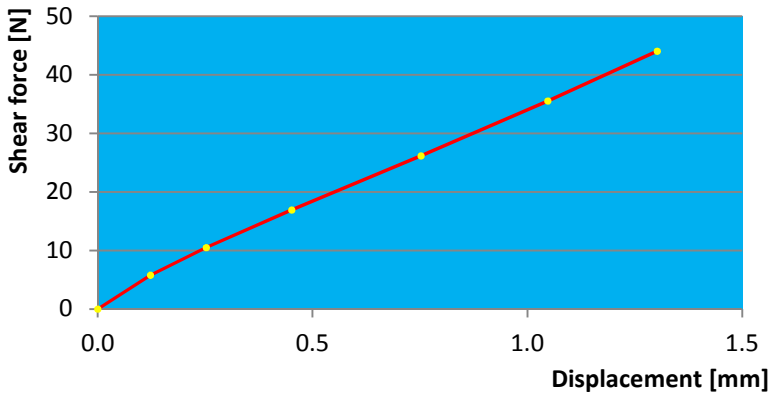

Figure 60: Shear force vs. displacement curve of the prosthesis under a combined load

Displacement [mm]	Shear force [N]
0.0000	0.000
0.1226	5.788
0.2525	10.496
0.4514	16.915
0.7522	26.158
1.0475	35.539
1.3020	44.044

Table 14: Displacement and shear force over the midplane of the inlay

In the previous image (*fig. 60*) can be seen that the relationship between displacement and shear force acting on the inlay is substantially linear.

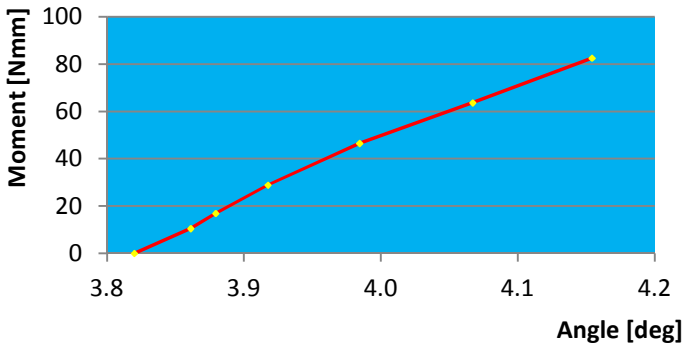

Figure 61: Moment vs. angle curve of the prosthesis under a combined load

Angle [deg]	Rotation [deg]	Moment [Nmm]
3.82	0.0000	0.000
3.86	0.0412	10.536
3.88	0.0594	16.931
3.92	0.0976	28.931
3.98	0.1645	46.556
4.07	0.2471	63.740
4.15	0.3342	82.608

Table 15: Angle, rotation and moment over the midplane of the inlay

The moment increases as the angle between the metal plates gets greater (*fig. 61*), as happened in the previous analysis; this is because of the bad position adopted by the inlay where both plates touch the inlay creating a torque that increases the moment on the midplane of the inlay (*fig 62*).

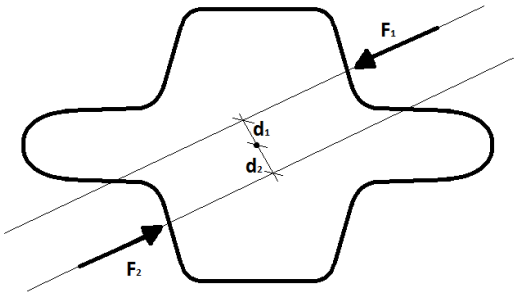

Figure 62: Diagram of the torque generated by the contacts

Where the central point is the center of rotation, F_1 and F_2 are the resulting loads from the plates and d_1 and d_2 are the perpendicular distance from the axis of rotation. In this case the resulting moment is $M_F = F_1 \cdot d_1 + F_2 \cdot d_2$

Comparison of the combined load analysis

First of all there is a result that must be commented, this is the main difference between the compressive load analysis which is the increment of the load and the distance between the metal plates as the shear load increases. This fact creates the first doubt about the proper functioning of the artificial disc.

	Right position [N/mm^2]	Bad position [N/mm^2]
Sx	0.849473 (t)	0.769492 (t)
Sy	0.629640 (t)	0.588437 (t)
Sz	0.587979 (c)	0.541490 (t)
Seqv	0.357023	0.367946

Table 16: Maximum stress values over the trabecular bone of the vertebra

Maximum stresses of the trabecular bone are found in the combined analysis of the disc in its correct position. Maximum Sx and Sy are located in the junction of the vertebral body with the pedicles and the maximum Sz is located in the pars interarticularis. In the other hand, the maximum equivalent stress is located in the junction of the vertebral body with the pedicles in the combined analysis with the disc in its bad position.

In any case, the stresses of the cancellous bone under these load state are not enough to damage the bone, which its ultimate state is about 8 MPa. But it is certainly that the spine is not under a critical load so probably if the load increases until the critical value the bone is going to get damaged in the places where the maximum is located.

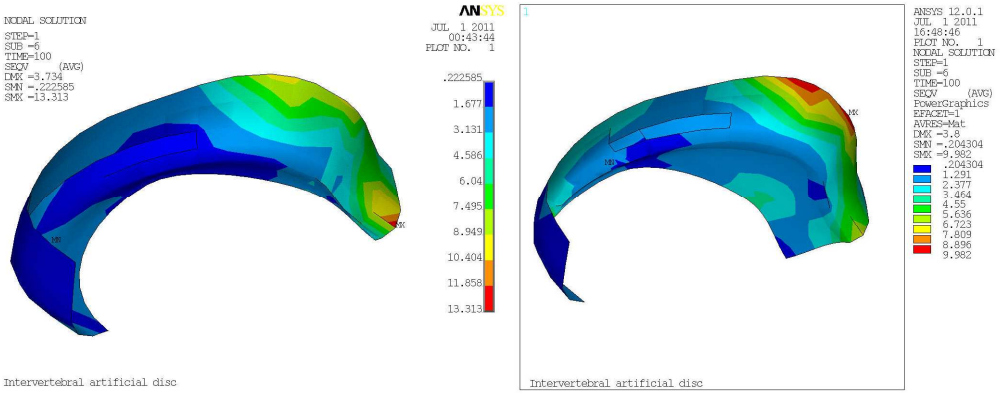

Figure 63: Von Mises stresses of the cortical bone in both disc positions.

As in the in the analysis under a compression load, the maximum tensile stresses of the cortical bone are located in the vertebral lamina. If the equivalent stresses of the cortical bone of the lower vertebral body are compared from one combined analysis to the other (*fig. 63*), can be observed that maximum stresses are found in the posterior-lateral part of the vertebral body.

In this case, both stress values are nearly the same. Like in the cancellous bone, stress values are not enough to damage the cortical bone which has an ultimate stress about 100 MPa.

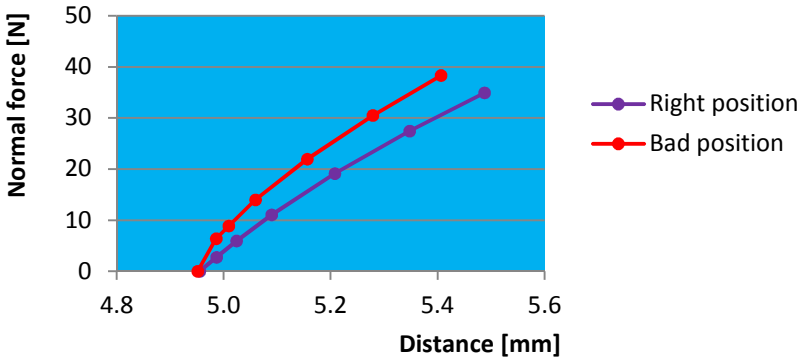

Figure 64: Normal force vs. distance curve of both combined analysis

In the previous graphic (*fig.64*) we can compare the disc behavior on the normal force. It can be observed that the behavior in both cases is substantially similar. It is important to clarify that the normal force values are higher in the analysis of the disc in its bad position because the vertical displacement applied to the upper nodes of the L3 is greater than the vertical displacement in the analysis of the disc in its good position.

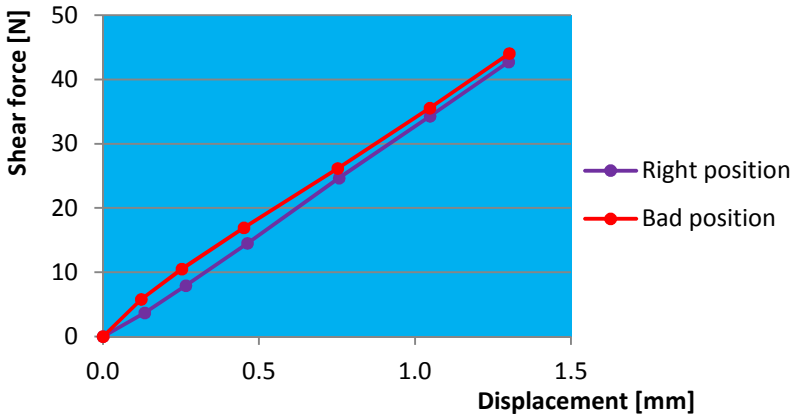

Figure 65: Shear force vs. distance curve of both combined analysis

As it can be seen in the previous graphic (*fig. 65*), in both cases, the shear behavior of the intervertebral disc is almost the same; both of them are substantially linear and are placed practically on the same place. This similar behavior is useful to ensure that the displacements applied to the upper nodes of the L3 in both cases were the correct ones.

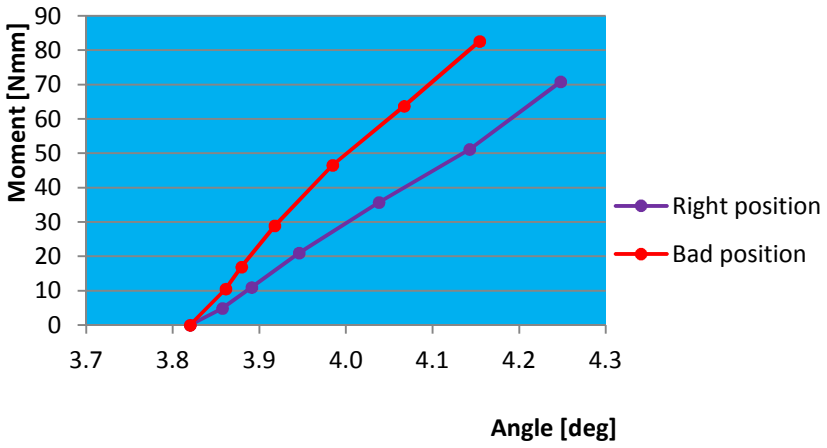

Figure 66: Moment vs. angle curve of both combined analysis

Like in the compression analysis, the moment experimented by the midplane of the inlay in the analysis of the artificial intervertebral disc in its bad position (*fig. 66*) is higher than the moment experimented by the inlay of the artificial intervertebral disc in its good position.

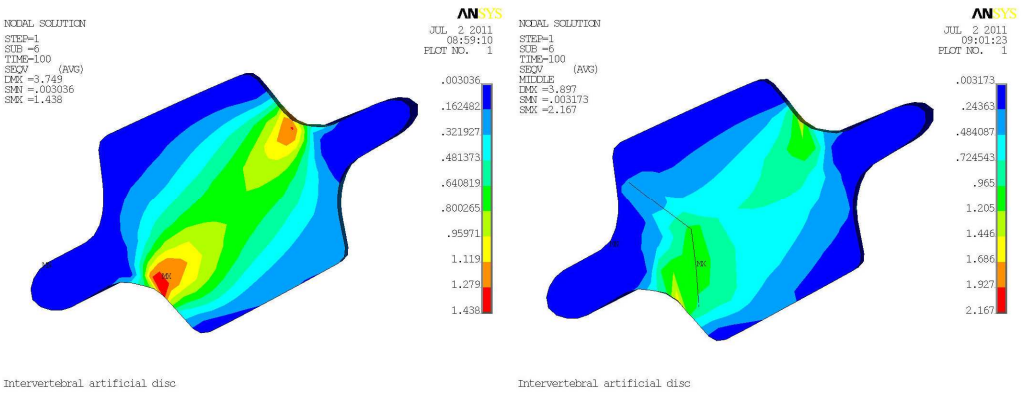

Figure 67: View of the Von Mises stresses of the inlay in the right and bad position analysis

As it can be observed in the value scale of the previous image (*fig. 67*), the maximum stresses of the inlay appears in the combined analysis of the intervertebral disc in its bad position reaching a maximum value of 2.167 MPa.

Conclusions

The vertebral spine is a complex structure which carries all the weight of the upper part of the body, because of this, there are a lot of tissues that provides its stability. These tissues are muscles, ligaments and special structures like the intervertebral discs. Due to many possible causes, these structures can be damaged. If an intervertebral disc is damaged and the conservative treatments are not useful to relieve pain, the only solution is the surgery. Most of the times this surgery consists in a replacement of the damaged intervertebral disc by a prosthesis which has the same behavior of the real disc. To achieve the same behavior of the intervertebral disc, the prosthesis must be analyzed under different load states.

In this project, an artificial intervertebral disc has been designed using APDL language. The values of the artificial intervertebral disc parameters have been chosen according to the model of the lumbar spine used to perform the analysis. In this case, we studied the response of an artificial disc with a thickness reduction of the inlay brim. The problem in the disc design is that the brims of the plates did not contact with the brim of the inlay. After the analysis of the prosthesis under a compressive load of the artificial disc in its good and bad position, we concluded that the stresses of the disc and the bones were not enough to damage them but as it was predicted the artificial intervertebral disc behavior was not the same as the real disc. The slope of the compressive force vs. distance was considerably different from the one of hyperelastic materials. The cause of this malfunction was because of the lack of contact between the inlay and plates brims, if they had been in contact, the stiffness of the hyperelastic had increased and the slope of the compressive force vs. distance had been greater as the curve of a hyperelastic material.

The results of the combined analysis were the most surprising, in both disc locations, while the load was applied, the distance between the plates and the angle of the metal plates increased. The shear load in both analyses had the same behavior, shear vs. displacement curves were substantially ate the same place. The fact that showed the malfunction of the disc was when under a shear load, the inlay rotate towards the anterior part of the vertebrae. This malfunction of the artificial intervertebral disc could create an instability and even the inlay of the prosthesis could have left the socket where it fits, being a serious risk to the patient due to the proximity of the common iliac artery and vein.

In this project, only two type of analysis have been done, but for sure to the spinal column is loaded in more other types of loads. Other analyses that will be useful to study the behavior of the disc are the ones that correspond to the multiple movements of the spinal column. These

movements are the flexion, the extension, the lateral flexion, the circumduction (combined flexion and/or extension with the lateral flexion), the axial rotation, the rotation in flexion and a pure shear load.

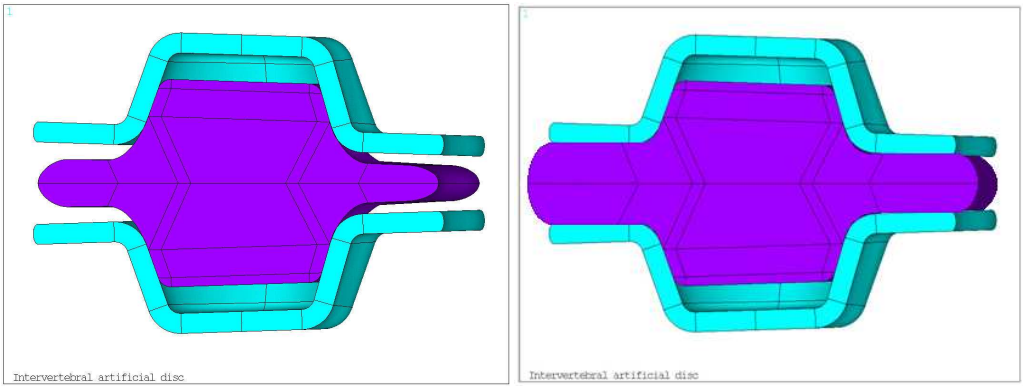

Figure 68: Current and improved design of the prosthesis

To conclude, we have to say that to achieve the properly operation of the prosthesis the inlay brim needs to have a greater thickness. If the inlay brim is reduced, the artificial disc will not work properly producing several instability problems and will become a dangerous device into the patient's body because may be more harmful than beneficial.

Image source

[1] http://www.medscape.com/viewarticle/405642_2

[2] NEUMANN, D.A. (2010). *Kinesiology of the Musculoskeletal System: Foundations for Rehabilitation.* 2nd ed. Mosby Elsevier, ISBN: 978-0-323-03989-5

[3] http://www.advancedorthopain.com/spine-anatomy3.html

[4] http://www.kxcad.net/ansys/ANSYS/ansyshelp/Hlp_G_MOD5_1.html

[5] ANSYS Element Reference, Release 12.1, November 2009

[6] http://en.wikipedia.org/wiki/Arruda-Boyce_model

[7] WANG, E. *Penalty vs. Lagrange: ANSYS contact*, CAD-FEM GmbH. Germany (online resource)

[8] http://www.engapplets.vt.edu/Mohr/java/nsfapplets/MohrCircles2-3D/Theory/theory.htm

[9] http://www.kxcad.net/ansys/ANSYS/ansyshelp/thy_tool10.html

[10] http://en.wikipedia.org/wiki/Common_iliac_artery

Bibliography

NEUMANN, D.A. (2010). *Kinesiology of the Musculoskeletal System: Foundations for Rehabilitation.* 2nd ed. Mosby Elsevier, ISBN: 978-0-323-03989-5

NORDIN, M.; FRANKEL, V.H. (2001). *Basic Biomechanics of the Musculoskeletal System.* 3rd ed. Lippincott Williams & Wilkins. ISBN: 0-683-30247-7

KAPANDJI, A.I. (1998). *Fisiologia articular (vol 3): Tronco y raquis.* Editorial Medica Panamericana. ISBN: 978-8-479-03376-7

BOGDUK, N.; ENDRES, S.M. (2005). *Clinical Anatomy of the Lumbar Spine and the Sacrum.* 4th ed. Churchill Livingstone, ISBN: 0-443-10119-1

WANG, E. *Penalty vs. Lagrange: ANSYS contact*, CAD-FEM GmbH. Germany

ANSYS Element Reference, Release 12.1, November 2009

ANSYS Modeling and Meshing Guide, Release 12.1, November 2009

ANSYS Structural Analysis Guide, Release 9.0, November 2004

ProDisc-L Total Disc Replacement: Technique Guide, Synthesis Spine, 2006

ANSYS Workbench – Mechanical Structural Nonlinearities, Chapter 6 (Hyperelasticity), 2009

Eijkelkamp M. F., van Donkelaar C. C., Veldhuizen A. G., van Horn J. R., Huyghe J. M.: *Requirements for an artificial intervertebral disc*, The International Journal of Artificial Organs 24:311-321, 2001.